Published in final edited form as:

Cell Metab. 2023 December 05; 35(12): 2200–2215.e9. doi:10.1016/j.cmet.2023.10.014.

Stress-induced β-cell early senescence confers protection against type 1 diabetes

Hugo Lee[1,*], **Gulcan Semra Sahin**[1,*], **Chien-Wen Chen**[2], **Shreyash Sonthalia**[1], **Sandra Marín Cañas**[3], **Hulya Zeynep Oktay**[1], **Alexander T. Duckworth**[1], **Gabriel Brawerman**[4], **Peter J. Thompson**[4], **Maria Hatzoglou**[2], **Decio L. Eizirik**[3], **Feyza Engin, Ph.D.**[1,5,6,7,**]

[1]Department of Biomolecular Chemistry, University of Wisconsin-Madison, School of Medicine and Public Health, Madison, WI 53706, USA.

[2]Department of Genetics and Genome Sciences, Case Western Reserve University, Cleveland, OH 44106, USA.

[3]ULB Center for Diabetes Research, Medical Faculty, Université Libre de Bruxelles, Campus Erasme, B-1070, Brussels, Belgium.

[4]Department of Physiology & Pathophysiology, Rady Faculty of Health Sciences, University of Manitoba, Winnipeg, MB, Canada.

[5]Department of Medicine, Division of Endocrinology, Diabetes & Metabolism; University of Wisconsin-Madison, School of Medicine and Public Health, Madison, WI 53705, USA.

[6]Department of Cell and Regenerative Biology, Wisconsin Institute for Discovery, University of Wisconsin-Madison, School of Medicine and Public Health, Madison, WI 53705, USA.

[7]Lead contact

SUMMARY

During the progression of type 1 diabetes (T1D), β-cells are exposed to significant stress and therefore require adaptive responses to survive. The adaptive mechanisms that can preserve β-cell function and survival in the face of autoimmunity remain unclear. Here we show that deletion of the unfolded protein response (UPR) genes, *Atf6α* or *Ire1α*, in β-cells of NOD mice prior to insulitis generates a p21-driven early senescence phenotype and altered β-cell secretome that significantly enhances leukemia inhibitory factor-mediated recruitment of M2

**To whom correspondence should be addressed: Feyza Engin, Ph.D. fengin@wisc.edu.
*These authors contributed equally to this work.

AUTHOR CONTRIBUTIONS

H.L. and G.S.S. designed and performed the experiments, analyzed the data, and wrote the manuscript. C.-W.C. analyzed HPAP data. Y.S. performed Ki67 staining. H.Z.O. contributed to IF staining of p21. A.T.D. helped with EMSA assay. S.M.C. performed experiments with EndoC-βH1 cells. G.B. performed CXCL14 ELISAs. P.J.T., M.H., and D.L.E. interpreted experiments and revised the manuscript. F.E. conceived, supervised and supported the project, designed experiments, interpreted results, wrote and revised the manuscript.

DECLERATION OF INTERESTS

The authors declare no competing interests.

macrophages to islets. Consequently, M2 macrophages promote anti-inflammatory responses and immune surveillance that cause resolution of islet inflammation, removal of terminally senesced β-cells, reduction of β-cell apoptosis, and protection against T1D. We further demonstrate that p21-mediated early senescence signature is conserved in residual β-cells of T1D patients. Our findings reveal a previously unrecognized link between β-cell UPR and senescence that, if leveraged, may represent a novel preventive strategy for T1D.

eTOC

Lee et al. show that β-cell-specific deletion of ATF6 and IRE1α in NOD mice prior to insulitis initiates early senescence, which alters β-cell secretome and induces M2 macrophage recruitment to the islets. M2 macrophages promote immune surveillance and removal of terminally senesced β-cells resulting in protection against type 1 diabetes.

Graphical Abstract

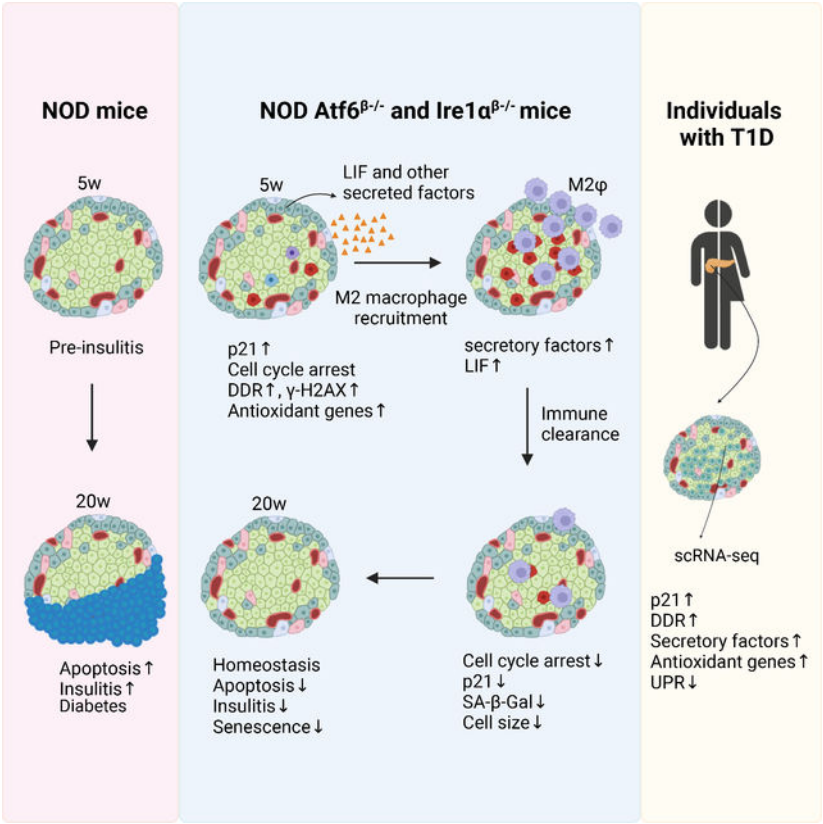

INTRODUCTION

Maintenance of cellular and organismal homeostasis under stress conditions is achieved by the activation of highly conserved cellular stress responses. The adaptive stress responses engage a network of signaling mechanisms to resolve the stress and re-establish cellular homeostasis, but persistent and/or excessive stress responses can be detrimental and lead to apoptosis. Cellular stress often affects multiple organelles simultaneously, triggering

multiple stress responses. The crosstalk among these stress responses, their coordinated regulation, and non-cell autonomous effects likely play a critical role in determining adaptive vs. maladaptive outcomes, but knowledge of the mechanisms involved in this crosstalk is limited.

One type of cellular stress is the endoplasmic reticulum (ER) stress that is caused by the accumulation of unfolded proteins inside the ER, viral infections, toxins, and chronic inflammation. ER stress triggers the unfolded protein response (UPR) to mitigate the stress and restore cellular homeostasis. The canonical UPR is mediated by activation of ER-membrane localized proteins inositol-requiring protein-1 (IRE1), protein kinase RNA-like ER kinase (PERK) and activating transcription factor-6 (ATF6). PERK attenuates translation of most mRNAs but also specifically induces translation of the transcription factor *Atf4*, which directs transcription of genes involved in amino acid metabolism and oxidative stress reduction.[1] IRE1α activation leads to a highly specific splicing reaction of XBP1 mRNA generating spliced XBP1, a transcription factor that regulates the expression of the UPR target genes including ER chaperones, ER-associated degradation (ERAD) components, and lipid biosynthetic enzymes. ATF6, upon undergoing proteolytic cleavage in Golgi, functions as an active transcription factor upregulating target genes encoding ER chaperones, ERAD components, and XBP1. While the UPR initially attempts to promote adaptation of the cells to ER stress, in the presence of prolonged or severe stress it induces a pro-apoptotic response that eliminates terminally stressed cells.[2,3]

Type 1 diabetes (T1D) results from insulin insufficiency owing to near complete destruction of insulin-producing pancreatic β-cells by an autoimmune process. Over the last decade, the active participation of pancreatic β-cells in their own autoimmune destruction and the impact of aberrant stress responses to T1D disease progression have gained considerable attention.[4–6] Early studies demonstrated that β-cells exposed to pro-inflammatory cytokines have significantly increased ER stress and UPR.[7,8] Preclinical and clinical studies provided further evidence for the presence of β-cell ER stress and dysregulated UPR long before the initiation of T1D.[9–12] Pharmacological mitigation of ER stress and inhibition of IRE1α activity prevented T1D in preclinical models.[9,13,14] However, the β-cell-specific functions of the other UPR sensors (ATF6 and PERK), the crosstalk between β-cells and immune cells, and the intricate relationship between ER stress and other cellular stress responses during autoimmune progression have remained largely unknown.[15]

Senescence is a stress response program of stable growth arrest mediated by cyclin-dependent kinase inhibitors such as $p21^{Cip1}$ and $p16^{Ink4a}$ and involves a variety of cellular changes, such as a prosurvival phenotype and a complex and dynamic secretome consisting of growth factors, cytokines, chemokines, and other factors known as the senescence-associated secretory phenotype (SASP).[16,17] The SASP elicits immune surveillance, leading to removal of senescent cells from tissues and restoration of homeostasis,[18–20] but when the immune system is compromised, such as during aging, senescent cells accumulate leading to tissue dysfunction.[21] Notably, senescent β-cells accumulate during the natural history of T1D in non-obese diabetic (NOD) mice and humans and contribute to disease progression, as small molecule targeting of senescence prevents T1D in NOD mice.[22] The accumulation of senescent β-cells with SASP in T1D suggests a defect or lack of immune surveillance, but

whether senescent β-cells elicit surveillance by the immune system has not been determined. Moreover, how senescence relates to other β-cell stress responses, such as the UPR, is not clear.

Here we show that deletion of key UPR mediators, *Atf6α* or *Ire1α*, in β-cells leads to an early senescence program driven by p21 resulting in a unique secretome that recruits M2 macrophages to islets. Consequently, M2 macrophage-mediated anti-inflammatory, immunosuppressive responses and immune surveillance result in markedly diminished terminally senesced β-cells, resolution of islet inflammation, reduction of β-cell apoptosis, and increased β-cell survival, leading to protection from T1D in NOD mice. Analysis of single cell transcriptomics data from human T1D islets and studies inhibiting ATF6 in human EndoC-βH1 cells and donor islets show that p21-mediated early senescence signature is also present in residual β-cells of T1D patients. Our work demonstrates a novel link between β-cell UPR and senescence in the restoration of islet homeostasis and attenuation of T1D.

RESULTS

Atf6 deletion in NOD β-cells protects against T1D

Previous reports show that while whole-body deletion of α and β isoforms of *Atf6* in mice leads to embryonic lethality,[23] β-cell-specific deletion of *Atf6α* on C57BL/6J background leads to mild glucose intolerance and a decrease in glucose-stimulated insulin secretion.[9] When crossed with a virally-induced diabetes mouse model, *Atf6α* deficiency in β-cells does not alter diabetes incidence.[9] To get insight into the role of β-cell ATF6 in T1D development, we generated β-cell-specific *Atf6α* knockout mice (Atf6$^{\beta-/-}$) on NOD background. To this end, we mated NOD Atf6$^{fl/fl}$ mice with NOD Ins2Cre^{ERT} mice.[13] The resulting Atf6$^{fl/fl}$; Ins2Cre^{ERT} mice were further mated with Atf6$^{fl/fl}$ mice. Of note, we had previously characterized the NOD Ins2Cre^{ERT} mice,[13] which gave rise to the non-littermate controls in this study. To achieve deletion of *Atf6* in β-cells prior to insulitis, we administered tamoxifen to all pups during P1–3 (Figure 1A). We confirmed β-cell-specific deletion of *Atf6* by co-staining pancreatic sections with anti-ATF6 and anti-insulin antibodies (Figure 1B). The quantitative PCR (qPCR) analysis showed a ~60% reduction of *Atf6* mRNA in the islets of Atf6$^{\beta-/-}$ mice (Figure 1C).

To determine the effects of *Atf6* deletion on diabetes progression in NOD mice, we measured the blood glucose levels of knockout, littermate floxed control, and Cre-only mice weekly from 3 to 50 weeks of age (Figure 1D). Remarkably, while ~55–65% of the floxed and Cre-only control mice became diabetic by 50 weeks, only 15% of the Atf6$^{\beta-/-}$ mice became diabetic, indicating a significant protective effect of loss of *Atf6* in β-cells (Figure 1E). The islets from Atf6$^{fl/fl}$ and Atf6$^{\beta-/-}$ mice showed normal morphological features at 10 weeks of age, as evaluated by immunofluorescence (IF) staining on pancreatic sections using anti-insulin and anti-glucagon antibodies, along with nuclear stain DAPI (Figure 1F), but there was a higher relative fluorescence intensity for insulin in islets of Atf6$^{\beta-/-}$ mice (Figure 1G). Serum insulin levels were also markedly increased in knockout mice compared to their littermate controls (Figure 1H), indicating preservation of β-cell functionality in Atf6$^{\beta-/-}$ mice. Histomorphometric analyses did not indicate any significant differences in

the average islet area of Atf6$^{fl/fl}$ and Atf6$^{\beta-/-}$ mice (Figure 1I). Taken together, these data demonstrate that deletion of β-cell *Atf6* prior to insulitis results in maintenance of β-cell function and reduced diabetes incidence in NOD mice.

Atf6$^{\beta-/-}$ mice exhibit markedly reduced insulitis

Atf6 activation induces proliferation of mouse and human β-cells under hyperglycemic conditions,[24] however, quantification of the percentage of Ki67^{+} β-cells in Atf6$^{\beta-/-}$ mice versus control animals did not reveal any significant differences at either 5 or 10 weeks of age (Figures 1J and 1K), suggesting no impact on proliferation. We then stained the cells with Annexin V, a marker of apoptosis, and propidium iodide (PI) and observed markedly decreased apoptosis in the islets of Atf6$^{\beta-/-}$ mice compared to control islets (Figures 1L and 1M), a finding that is in line with the reduced diabetes incidence phenotype (Figure 1E).

Infiltration of islets by immune cells, insulitis, is a hallmark of T1D, hence we asked if loss of *Atf6* in β-cells affected islet immune infiltration. Hematoxylin and eosin (H&E) staining of pancreatic sections from 10 weeks of age Atf6$^{fl/fl}$ and Atf6$^{\beta-/-}$ mice revealed that knockout mice had notably less islet immune cell infiltration (Figure 1N). Both aggressive and non-aggressive insulitis were markedly diminished in the pancreata of Atf6$^{\beta-/-}$ mice, as evaluated by insulitis scoring (Figure 1O), whereas the percentage of insulitis-free intact islets was significantly increased (38% vs. 68%, $p<0.05$) in Atf6$^{\beta-/-}$ mice (Figure 1P). These results indicate that the extent of invasive islet immune infiltration was markedly diminished in the pancreata of Atf6$^{\beta-/-}$ mice, which is reflected in their increased serum insulin levels, preserved islet architecture, and significantly decreased diabetes incidence.

We next investigated the impact of the observed β-cell protection on the distributions and proportions of immune cell populations involved in T1D pathogenesis. Immunophenotyping by flow cytometry of pancreata, spleen, and pancreatic lymph nodes (PLNs) of 12-week-old control and knockout mice revealed no significant differences in the relative representation of effector T cells, B cells, regulatory T cells, and dendritic cells (Figures 1Q–1S and S1A–S1L). There was only a non-significant ($p>0.05$) trend towards a decreased percentage of macrophages in the pancreata of Atf6$^{\beta-/-}$ mice (Figure 1Q) when cells were stained for the pan-macrophage marker F4/80. These results suggest that while the distribution of immune cell populations remain unaltered, better islet function and survival might have reduced recruitment of immune cells to the islets of Atf6$^{\beta-/-}$ mice, reflected in reduced insulitis.

Compromised UPR induces senescence

Next, we performed RNA sequencing (RNA-seq) on sorted β-cells from 6-week-old control and knockout mice to gain insight into the underlying mechanisms of diabetes protection in Atf6$^{\beta-/-}$ mice. We used a modified version of a previously described protocol,[25] which allowed us to obtain high quality RNA from sorted β-cells (Figures S2A–S2E). Differential expression analysis of Atf6$^{\beta-/-}$ and Atf6$^{fl/fl}$ β-cells with EdgeR at false discovery rate (FDR) <0.05 identified 698 differentially expressed genes (Figures S2F and S2G). KEGG pathway analysis revealed 17 enriched pathways (pBonf<0.05), of which the top one was the p53 signaling pathway (p value of 0.008) (Figure S2H). Of note, expression of several genes in the p53 signaling pathway *(Mdm2, Sfn, Ccng1, Cdkn1a,*

Cd82, Zmat3, Ccnd1), which play important roles in regulation of the cell cycle and cell survival, were substantially upregulated in β-cells of Atf6$^{\beta-/-}$ mice (Figure 2A). Interestingly, we detected a significant increase in the expression of *Nrf2 (Nfe2l2)*, a master regulator of antioxidant, anti-inflammatory and other cytoprotective mechanisms, and genes that are directly regulated by *Nrf2 (Gpx3, Gstp1, Gstm2, Hmox1, Txnrd1, Gclc)* in β-cells of Atf6$^{\beta-/-}$ mice (Figure 2B). The p53/21 signaling can regulate several different cell stress responses including oxidative stress and the DNA damage response (DDR).[26] Hence, we examined the expression of DDR genes and observed several of these markers to be differentially expressed in β-cells of Atf6$^{\beta-/-}$ mice (Figure 2C). To determine if this intriguing phenotype was unique to the ATF6 branch of the UPR, we focused on another UPR sensor, IRE1α. We reanalyzed our single-cell RNA sequencing (scRNA-seq) dataset from Ire1α$^{\beta-/-}$ mice[13] and observed that markers of these pathways were also substantially upregulated in β-cells of Ire1α$^{\beta-/-}$ mice (Figures 2D–2F). Despite these similarities, the striking morphological differences between Atf6$^{\beta-/-}$ and Ire1α$^{\beta-/-}$ islets led us to investigate the possibility of β-cell dedifferentiation in Atf6$^{\beta-/-}$ mice at the molecular level. The analysis of RNA-seq data for the expression of β-cell markers (Figures S2I), disallowed genes (Figure S2J), and dedifferentiation markers (Figure S2K) indicated comparable gene expression levels between control and knockout mice. Together with our histological findings indicating unaltered islet architecture and cellular composition, lack of insulin^{+}/glucagon^{+} bihormonal cells and normal insulin/glucagon staining pattern (Figure 1F), these data support the lack of β-cell dedifferentiation in Atf6$^{\beta-/-}$ mice.

The significant upregulation of *Cdkn1a* (that encodes for p21) and of DDR genes hinted at alterations in the cellular senescence program, as senescent β-cells show upregulation of p21 at the mRNA and protein levels in NOD mice and human islets.[22,27] Since mRNA levels do not necessarily reflect protein levels, we investigated the protein expression of senescence markers. P21 was markedly increased in β-cells of Atf6$^{\beta-/-}$ mice at 5 and 10 weeks of age, but it returned to basal levels at 20 weeks (Figures 2G and 2H). In addition to Atf6$^{\beta-/-}$ mice, we investigated the protein levels of p21 in β-cells of Ire1α$^{\beta-/-}$ mice and observed a significant increase in p21 at 5 weeks which gradually decreased at 12 and 24 weeks but remained significantly higher compared to control mice (Figures 2I and 2J).

The phosphorylation of the histone H2A member X (γ-H2AX) is a key step in the DDR.[28] γ–H2AX is often present in senescent cells due to accumulated DNA damage,[16] and also marks senescent β-cells in NOD mice and in genetic models of diabetes that involve β-cell senescence.[22,29,30] We detected a gradual increase in γ–H2AX levels in β-cells of Atf6$^{\beta-/-}$ mice (Figures 2K and 2L). γ–H2AX levels were also elevated in β-cells of 5-week-old Ire1α$^{\beta-/-}$ mice but returned to control levels at 12 weeks of age (Figures 2M and 2N). Another important feature of senescent cells is cell cycle arrest. We examined the cell cycle progression in the islets of Atf6$^{\beta-/-}$ and Ire1α$^{\beta-/-}$ mice by flow cytometry. At 6 weeks of age, the percentage of islet cells in G_0/G_1 phase was markedly decreased in both knockout models, while the percentage of knockout cells in G_2/M phase was substantially increased, suggesting a cell cycle arrest at this stage (Figures 2O–2Q). Taken together, these findings provide strong evidence that UPR-deficient (throughout the text this refers to specific loss of ATF6 and IRE1α sensors but does not include the PERK arm of the UPR) β-cells exhibit features of cellular senescence.

p21 is important for β-cell survival

The increase in p21 expression in both Atf6$^{\beta-/-}$ and Ire1α$^{\beta-/-}$ mice led us to further investigate the biological significance of p21 in Atf6$^{\beta-/-}$ mice. To this end, we exposed isolated islets from control and knockout mice to a chemical inhibitor of p21, UC2288,[31] and confirmed the efficacy of this inhibition via western blot (Figures S3A and S3B). P21 inhibition resulted in reduced expression of NRF2, a known target of p21, in the islets of Atf6$^{\beta-/-}$ mice (Figures S3A and S3C). The apoptosis marker cleaved Caspase-3 was markedly upregulated upon inhibition of p21 both in control and knockout islets (Figures S3A and S3D), suggesting that p21 plays a key role in islet cell survival during stress.

To complement this *ex vivo* study, we investigated the impact of genetic inhibition of p21 on diabetes incidence in the Ire1α$^{\beta-/-}$ mouse model. To this end, we injected 3-week-old Ire1α$^{\beta-/-}$ mice with either an adeno-associated virus targeting β-cell p21 or a control virus (Figures S3E and S3F). By 20 weeks of age, while AAV8-shScramble-injected Ire1α$^{\beta-/-}$ mice exhibited approximately 25% diabetes incidence, AAV8-RIP-shp21-injected mice showed more than 75% diabetes incidence supporting the notion that p21 is important for β-cell survival (Figure S3G). Taken together, these data suggest that maintaining p21 levels is important for β-cell survival and that elevated p21 levels in β-cells can lead to diabetes prevention or recovery[32] in T1D animal models.

UPR sensors differentially regulate p21

Next, we investigated the molecular mechanisms by which the UPR regulate p21 expression. Analysis of the *Cdkn1a* promoter revealed a consensus cyclic AMP (cAMP) response element (CRE) (Figure 3A).[33] CRE binding protein (CREB) binds to the CRE element on the promoter of several genes and activates them. ATF6 has been previously shown to inhibit CREB-dependent transcription of gluconeogenic enzymes,[34] and we asked whether *Cdkn1a* upregulation in the absence of ATF6 is CREB-dependent. Co-treatment of a rat insulinoma cell line, INS1 832/3, with the ER stressor tunicamycin and an ATF6 inhibitor, Ceapin-A7,[35] led to significant upregulation of *Cdkn1a* mRNA levels, while CREB inhibition by the specific inhibitor 666–15[36] suppressed *Cdkn1a* mRNA and protein expression induced by ATF6 inhibition (Figures 3B–3D). Moreover, treatment of INS1 832/3 cells with forskolin, which stimulates CREB activity, significantly increased p21 at both mRNA and protein levels (Figures 3E–3G). Together, these data support the hypothesis that ATF6 suppresses *Cdkn1a* expression in a CREB-dependent manner (Figure 3H). To address this directly, we performed an electrophoretic mobility shift assay (EMSA) (Figures 3I–3J). Using an oligo containing the consensus CRE sequence as our positive control, we detected a robust shift when incubated with nuclear extracts from forskolin-treated INS1 832/3 cells. The same shift was observed upon forskolin treatment with the oligo containing *Cdkn1a* CRE element, consistent with previous reports showing CREB's direct binding to the *Cdkn1a* promoter.[37,38] On the other hand, nuclear extracts from cells transfected with constitutively active ATF6 before forskolin treatment decreased the *Cdkn1a* oligo shift. To eliminate the possibility that transfection alone was causing this decrease, we overexpressed GFP as a control and did not observe any effect. Furthermore, we observed that while excess cold *Cdkn1a* oligos competed to decrease the shift, excess cold *Cdkn1a* oligo containing mutations in CRE site did not do so. In addition, mutated *Cdkn1a* oligo did not induce a

shift in the presence of forskolin treatment (Figures 3I–3J). To verify the EMSA findings, we performed chromatin immunoprecipitation (ChIP) of p-CREB followed by qPCR for *Cdkn1a* promoter in INS1 832/3 cells. We observed that while forskolin treatment increased binding of p-CREB to its canonical target, *Sik1*, and to *Cdkn1a* promoter, overexpression of constitutively active ATF6 decreased the binding of p-CREB to *Sik1* and *Cdkn1a* promoter (Figure 3K). Taken together, these findings indicate that ATF6 blocks CREB-dependent transcription of *Cdkn1a*.

In addition to the CRE element, we identified a highly conserved unfolded protein response element (UPRE) (TGACGTG), a target sequence for spliced XBP1 (sXBP1),[39] on the *Cdkn1a* promoter (Figure 3L). This led us to evaluate whether the IRE1α/sXBP1 axis of the UPR regulates *Cdkn1a* directly. First, we confirmed specific immunoprecipitation of endogenous sXBP1 in INS1 832/3 cells (Figure 3M). Next, we performed ChIP of sXBP1 followed by qPCR for the sXBP1 canonical target, *Hspa5*, and *Cdkn1a* promoter regions. While the *Cdkn1a* promoter region containing CRE site was enriched following sXBP1 ChIP, the 3'UTR region of *Cdkn1a* was not, suggesting that sXBP1 directly binds to and regulates *Cdkn1a* expression (Figures 3N and 3O). Collectively, these data indicate the presence of direct and indirect regulation of p21 expression by two different UPR sensors.

Early senescence increases M2 macrophage recruitment

To further elucidate the mechanisms of β-cell survival upon UPR deficiency, we utilized an *in vitro* cell culture system and performed a transwell migration assay (Figures S4A and S4B). Treatment of NOD mouse-derived NIT1 cells with Ceapin-A7 resulted in upregulation of the early senescence marker p21 (Figure S4C). Since p21 is known to drive a unique secretome in early senescent cells known as the p21-associated secretory phenotype (PASP),[20] we next investigated PASP markers in NIT1 cells. Consistent with increased p21 levels, we detected substantially increased expression of PASP markers when cells were treated with Ceapin-A7 (Figure S4C). Next, we examined proliferation, which was reduced in a DNA damage model of senescence in NIT1 cells.[27] In agreement with this, we identified significantly reduced $Ki67^{+}$ cells when treated with Ceapin-A7 (Figures S4D and S4E), while we did not detect any difference in apoptosis (Figures S4F and S4G). These data suggest that Ceapin-A7-treated NIT1 cells can mimic some aspects of cellular senescence and allow us to explore the mechanisms by which p21-mediated signaling affects β-cell survival.

The PASP markers were recently identified in senescence-induced mouse embryonic fibroblast (MEF) cells.[20] Using the PASP gene list from this study along with our own RNA sequencing data from $Atf6^{\beta-/-}$ and $Ire1\alpha^{\beta-/-}$ mice, we identified 23 markers that form the "core" PASP markers in the UPR-deficient mice (Figure 4A). These markers included S*erpin1a, Ache, Gdf15, Pamr1, Ltbp2, Ptprg, and Cd81* (Figure 4B and Table S1). Analysis of our datasets revealed a remarkable increase in the expression of cytokines and chemokines associated with macrophage recruitment (Figures 4C and 4D). This raised the possibility that UPR deficiency could alter the PASP phenotype and consequently impact the migratory behavior of macrophages. To test this possibility, we used peritoneal immune cells of NOD mice and showed that conditioned medium from Ceapin-A7-treated NIT1

cells promoted migration of macrophages in a transwell system (Figures S4H and S4I). The migration of the suspended cells (lymphocytes), on the other hand, was not affected by the conditioned medium (Figure S4J).

These *in vitro* findings led us to examine whether islet infiltration by macrophages was altered in the UPR-deficient mice. Macrophages play a significant role in T1D etiology[40] and play a pivotal role in initiation and perpetuation of the disease. Macrophages are classified as proinflammatory "classically activated" (M1) cells and anti-inflammatory "alternatively activated" (M2) cells. Because our UPR-deficient models were protected from diabetes, we hypothesized that PASP might lead to increased recruitment of M2 macrophages to the islets of Atf6$^{\beta-/-}$ and Ire1$\alpha^{\beta-/-}$ mice. To test this, we co-stained pancreatic sections from UPR-deficient models for Arginase1, a prototypic M2 macrophage marker,[41] and insulin. Quantification of the IF images revealed a striking increase in the number of Arginase1-positive M2 macrophages in the islets of Atf6$^{\beta-/-}$ (Figures 4E and 4F) and Ire1$\alpha^{\beta-/-}$ mice (Figures 4G and 4H) compared to control animals. Next, we investigated the distribution of M1 and M2 macrophages in the PLN and pancreata of Atf6$^{\beta-/-}$ and Ire1$\alpha^{\beta-/-}$ mice via flow cytometry. While there were no marked differences in the percentages of M1 and M2 macrophages in PLN, we detected significantly less M1 and substantially more M2 macrophages in the pancreata of Atf6$^{\beta-/-}$ and Ire1$\alpha^{\beta-/-}$ mice (Figures 4I–4L).

To investigate whether p21 plays a role in macrophage recruitment, we inhibited p21 in NIT1 cells using UC2288 in the presence or absence of Ceapin-A7 (Figure S4K). Pharmacological inhibition of p21 significantly diminished the migration of macrophages induced by Ceapin-A7 (Figures S4L and S4M). In line with this, we also detected significantly reduced M2 macrophage infiltration in the islets of Atf6$^{\beta-/-}$ and Ire1$\alpha^{\beta-/-}$ mice that underwent AAV8-mediated shp21 knockdown compared to control animals. (Figures 4M and 4N). These data support the hypothesis that p21 upregulation contributes to islet M2 macrophage recruitment in UPR-deficient mice.

The PASP component chemokine CXCL14 was shown to impact M1 macrophage polarization and contribute to mounting a cytotoxic T cell response to eliminate target cells.[20] Given that PASP alters the macrophage phenotype, we examined the secreted CXCL14 levels in conditioned medium of Ceapin-A7-treated NIT1 cells or cultured islets from Atf6$^{fl/fl}$ and Atf6$^{\beta-/-}$ mice. Our results indicate that the CXCL14 levels were low and therefore unlikely to have any biological impact under these *in vitro* and *ex vivo* conditions (Figures S4N and S4O).

Next, we investigated the chemokines that may have contributed to the increased macrophage recruitment. We identified that leukemia inhibitory factor (LIF), a well-established macrophage attractant,[42] was markedly upregulated in β-cells of both Atf6$^{\beta-/-}$ and Ire1$\alpha^{\beta-/-}$ mice (Figures 4C and 4D). Therefore, we probed the role of LIF in macrophage migration. Addition of anti-LIF neutralizing antibody to conditioned media from Ceapin-A7-treated NIT1 cells significantly blocked macrophage migration, unlike addition of control IgG (Figure 4O). Next, we investigated the role of LIF in M2 macrophage recruitment *in vivo*. To this end, we administered Atf6$^{\beta-/-}$ and Ire1$\alpha^{\beta-/-}$

mice with either IgG or anti-LIF antibody and analyzed M2 macrophage infiltration by IF. Remarkably, LIF inhibition significantly reduced M2 macrophage infiltration to Atf6$^{\beta-/-}$ and Ire1α$^{\beta-/-}$ islets (Figures 4P and 4Q).

To identify whether p21 is directly involved in regulation of LIF expression, we inhibited p21 in NIT1 cells. While ATF6 inhibition increased LIF expression, p21 inhibition almost completely attenuated this increase, supporting the notion that p21 acts upstream of LIF and regulates its expression in NIT1 cells (Figures 4R and 4S). Taken together, these data suggest that when β-cell UPR is compromised in the early stages of T1D, an early senescence mechanism is triggered. This transient senescence, through its unique secretome, augments M2 macrophage recruitment to the islet microenvironment and diminishes inflammation.

β-cell terminal senescence is reduced in UPR-deficient NOD mice

Our findings of early senescence inhibiting insulitis contrast with late senescence (terminal senescence) of β-cells that contributes to T1D pathogenesis.[22] This motivated us to test if early senescence leads to reduced late terminal senescence development and, consequently, attenuated disease progression. Therefore, we investigated the β-cell terminal senescence phenotype in UPR-deficient mice. One of the hallmarks of terminal/late senescence is permanent cell cycle arrest.[43] Hence, we analyzed cell cycle progression in the islets of Atf6$^{\beta-/-}$ and Ire1α$^{\beta-/-}$ mice. At 12 weeks of age, the percentage of islet cells in G_0/G_1 phase was markedly decreased while the percentage of cells in G_2/M phase remained significantly higher in Atf6$^{\beta-/-}$ mice. At 16 weeks of age, while the percentage of islet cells in G_0/G_1 phase was decreased in Atf6$^{\beta-/-}$ mice, cells in G_2/M phase in knockout animals were no longer significantly different from control cells (Figures 5A and 5B). Indeed, the population of islet cells observed in the G_2/M phase of Atf6$^{\beta-/-}$ mice at 16 weeks was substantially reduced when compared to 6 weeks of age Atf6$^{\beta-/-}$ mice (5.3% vs 10.2%) (Figures 2O and 2P). Similarly, Ire1α$^{\beta-/-}$ mice at 16 weeks of age no longer presented significant changes in the percentage of cells in G_0/G_1 or G_2/M phases as compared to controls (Figure 5C). The percentage of cells in G_2/M phases was markedly reduced in Ire1α$^{\beta-/-}$ at 16 weeks of age when compared to 6 weeks of age (1.3% vs 4.2%) (Figure 2Q), suggesting that either most knockout cells escaped the cell cycle arrest in these models, or that terminally senesced β-cells were cleared from the islet microenvironment.

To further investigate whether UPR-deficient mice have less terminally senescent β-cells as they age, we measured senescence-associated β-galactosidase (SA-β-gal) activity. SA-β-gal expression is widely used as a biomarker of terminal senescence.[43] C_{12}FDG is a substrate that is cleaved by SA-β-gal to produce a fluorescent product and serves as a surrogate marker for SA-β-gal activity. While we did not detect any changes at 5 weeks of age, we observed significantly reduced SA-β-gal activity in the islets of 20-week-old Atf6$^{\beta-/-}$ mice compared to control animals (Figures 5D and 5E). Ire1α$^{\beta-/-}$ mice at 20 weeks of age also showed substantially decreased SA-β-gal activity than control mice (Figures 5F and 5G). Another characteristic feature of senescent cells is an enlarged morphology; therefore, we assessed the size of islet cells in Atf6$^{\beta-/-}$ and Ire1α$^{\beta-/-}$ mice at different timepoints. While there was no marked change in cell size at 5-week-old Atf6$^{\beta-/-}$ mice, 20-week-old

Atf6$^{\beta-/-}$ and Ire1α$^{\beta-/-}$ mice exhibited significantly reduced cell size compared to their control littermates (Figures 5H–5K). Altogether, these data suggest that terminal senescence is markedly diminished in β-cells of the UPR-deficient NOD mice. These data also suggest that senescence induced by compromised UPR early in disease progression is different than the senescence detected in β-cells of aged NOD mice. The cells that are undergoing early senescence do not show typical features of terminal senescence such as increased cell size or SA-β-gal activity. Hence, we propose this state of senescence as an acute state which leads to immune surveillance by M2 macrophages and removal, while their non-senescent counterparts are subsequently protected from autoimmune destruction.

P21 early senescence signature is conserved in human T1D

To examine whether loss of the UPR impacts human β-cells similarly to NOD mice, we treated a human β-cell line, EndoC-βH1, with Ceapin-A7 in the presence or absence of tunicamycin. Inhibition of ATF6 resulted in significantly increased mRNA expression of *CDKN1A* and markers of PASP (Figure 6A). In agreement with this, treatment of islets from human donors (Table S2) with Ceapin-A7 and IRE1α/XBP1 inhibitor, 4μ8C, showed markedly increased expression of *CDKN1A* and markers of PASP (Figure 6B). Next, we explored the expression of these markers in residual β-cells of individuals with T1D using scRNA-seq dataset produced by the Human Pancreas Analysis Program (HPAP)[44] (Table S3). Remarkably, we found that markers of the p53/p21 pathway, antioxidant response, DDR, and PASP that we identified in our animal models, were significantly upregulated in β-cells of T1D donors (FDR<0.05) (Figures 6C–6F). These data suggest that upregulation of conserved adaptive responses in residual β-cells of T1D donors may have contributed to their escape from autoimmune attack. It also suggests that these responses were not sufficient to preserve β-cell function as observed in UPR-deficient mice, likely due to insufficient immune clearance and the presence of persistent inflammatory environment in human islets.

DISCUSSION

Our current knowledge of ATF6 functions comes from its prosurvival homeostatic functions on ER proteostasis. While its function in β-cells is still under investigation, evidence suggests that ATF6 can promote β-cell survival and proliferation during the adaptive stress response.[24,45,46] The present study reveals, for the first time, a novel and key role for β-cell ATF6 in T1D. Atf6$^{\beta-/-}$ mice show significantly reduced diabetes incidence. This phenotype resembles *Ire1α* knockout mice on NOD background,[13] although with some differences. First, NOD Ire1α$^{\beta-/-}$ mice show transient dedifferentiation that Atf6$^{\beta-/-}$ mice do not exhibit. Second, Ire1α$^{\beta-/-}$ mice have a greater degree of diabetes protection. Third, unlike the observations in Ire1α$^{\beta-/-}$ mice,[13] we did not detect a significant reduction in the percentage of CD8^{+} T cells in pancreata of Atf6$^{\beta-/-}$ mice, albeit this could be due to the differences in time point that was chosen for the analysis in these mice or differences in the milieu of antigens presented by β-cells in these models.

How does losing specific UPR sensors prior to insulitis lead to β-cell survival? What is the reason for the induction of multipronged stress responses in UPR-deficient NOD

mice? One possibility is that ATF6 and IRE1α hyperactivity during early stages of disease leads to increased transcriptional burden in the ER and, consequently, exacerbates stress in β-cells of NOD mice which are already fragile.[47] Hence, deletion of these sensors during this stage could be beneficial. Another plausible explanation would be that mild stress induced by deletion of the UPR sensors results in engagement of a "hormetic" response.[48,49] Hormesis is a phenomenon in which a low level of stress stimulates stress adaptation that enhance cellular and organismal health and render them resilient to a subsequent and more severe stress. Hence, the activation of early senescence response and subsequent immune surveillance, along with the antioxidant response and DDR, can all be an integral part of a hormetic response to achieve resolution of stress and re-establishment of homeostasis.

While the continuous accumulation of senescent cells compromises tissue function, a short-term SASP triggers immune-mediated clearance of these senescent cells, therefore preventing persistent accumulation of senescence-induced signals and re-establishing tissue homeostasis.[20,50] Indeed, transient senescence plays an important role in development, wound healing, regeneration, and tissue repair.[50–59] These examples suggest that the duration and timing of the senescence program may be the major determinants of its adaptive outcomes, a phenomenon also observed in other stress responses, including the UPR.

Our results suggest that early senescence, induced by selective loss of UPR signaling in NOD mice, promotes high levels of islet infiltration by M2 macrophages. The role of M2 macrophages in NOD mice was previously investigated and it was shown that adoptive transfer of M2 macrophages to prediabetic NOD mice was sufficient to prevent T1D.[60] This protective effect was mostly attributed to the immunosuppressive functions of M2 macrophages, however, whether removal of senescent β-cells also contributed to diabetes protection have remained unknown. Additionally, the M2 polarization process was shown to be less effective in T1D patients than in healthy subjects depending on the stage of disease.[61] While monocytes of new-onset T1D children were still able to differentiate into M2 macrophages, this process and the ability of these cells to produce anti-inflammatory IL-10 were significantly limited in long-standing T1D patients.[61]

Accumulating evidence suggest that once recruited, macrophages can clear senescent cells, allowing for regeneration and repair of the damaged tissue.[18,62–64] Senescent hepatic stellate cells secrete a SASP that attracts macrophages,[65] and promote M1 macrophage polarization. M1 macrophages then eliminate senescent cells and support an antitumor microenvironment.[66] The SASP secreted by senescent thyroid cells skews macrophage polarization toward M2 phenotype.[67] These data suggest that depending on the cell type and context, macrophage polarization might be differentially affected by SASP. In line with this, our data showing reduced M1, but increased M2 macrophage populations in the pancreata of UPR-deficient mice suggest that not only the recruitment but also the polarization of macrophages might be affected in these models. Consequently, these findings support that M2 macrophages are likely to mediate the clearance of senescent β-cells leading to reduced terminal/late senescence in UPR-deficient NOD mice.

Human and mouse β-cells show different characteristics that often limit the translational efficacy of preclinical findings. Using IF assay[9] and scRNA-seq analysis,[68] we previously showed significantly diminished ATF6 protein and mRNA levels in β-cells of individuals with T1D. Our previous scRNA-seq analysis also revealed markedly reduced expression of the adaptive UPR transcriptomes in human T1D β-cells.[68] Interestingly, we observed a similar protective stress signature in β-cells of T1D donors that we identified in UPR-deficient NOD mice suggesting that, at least in part, the early senescence mechanisms are present and might have contributed to β-cell survival in the face of protracted autoimmunity in these individuals. While there is a growing interest in T1D clinical studies to inhibit harmful stress responses, we propose that enhancing adaptive responses during early stages of disease may present an alternative approach to help prevent β-cell immune destruction.

Limitations of study

Our current breeding scheme does not allow us to obtain the littermate control mice expressing Cre transgene alone. Although we confirmed that Cre transgene levels in these mice did not differ from knockout mice,[13] and Cre transgene did not alter diabetes progression and pathology in NOD mice, we still consider this as a limitation. Additionally, we did not demonstrate that M2 macrophages selectively phagocytose senescent β-cells or the specific receptors involved in such a process. Thus, it remains to be formally established whether M2 macrophages or other immune cells are responsible for the elimination of senescent β-cells in these models. Lastly, it is also possible that other mechanisms involving macrophages might have contributed to the observed phenotype.

STAR METHODS

RESOURCE AVAILABILITY

Lead Contact—Further information and requests for resources and reagents should be directed to and will be fulfilled by the lead contact, Feyza Engin (fengin@wisc.edu).

Materials availability—This study did not generate new unique reagents.

Data and code availability

- The RNA-seq data reported in this publication have been deposited in the NCBI Gene Expression Omnibus (GEO) (GSE239947). Uncropped western blots and source data can be found in Data S1.
- This paper does not report original code.
- Any additional information required to reanalyze the data reported in this paper is available from the lead contact upon request.

EXPERIMENTAL MODEL AND SUBJECT DETAILS

Mouse Lines and Tamoxifen Injections—The animal care and experimental procedures were carried out in accordance with the recommendations of the National Institutes of Health Guide for the Care and Use of Laboratory Animals. The protocol (#M005064-R01-A03 by F.E. for mice) was approved by the University of Wisconsin-

Madison Institutional Animal Care and Use Committee. Female NOD/ShiLtJ mice were purchased from Jackson Laboratory and housed under a 12:12-hr light/dark cycle, with unrestricted access to food and drinking water in an animal housing facility accredited by the Association for Assessment and Accreditation of Laboratory Animal Care. ATF6α floxed mice were a gift from Dr. Gökhan Hotamisligil (Harvard University, USA). Ins2-Cre^{ERT} mice were a gift from Dr. Douglas Melton (Harvard University, USA). IRE1α floxed mice were a gift from Dr. Iwawaki (Riken, Japan). Mice were backcrossed to NOD background more than 20 times. The genetic backgrounds of all intercrossed mouse models were verified by Jackson Laboratory's Genome Scan Service and the congenicity was reported as 100%.

To induce Cre recombinase activity, tamoxifen (T5648; Sigma-Aldrich) was dissolved in sterilized corn oil (C8267; Sigma-Aldrich) by shaking overnight in a 37°C incubator. The solution was protected from light. For IRE1α$^{fl/fl}$,IRE1α$^{fl/fl}$; Ins2Cre$^{ERT/+}$, and Cre^{+} mice, 10 mg/mL tamoxifen was administered to lactating mothers, beginning the day after delivery via intraperitoneal injection twice every 24 hours in five consecutive days as previously described.[13] To delete ATF6, 1 mg/mL tamoxifen was given once daily via daily intragastric injections to all newborn pups during P1–3 (including control and knockout mice). Animals were observed daily for health status, and any mice that met IACUC criteria for euthanasia were immediately euthanized. Weekly blood glucose measurements were performed after 6 hours of fasting through the tail tip using a CONTOUR Next glucometer (Ascensia) with CONTOUR Next test strips (Ascenscia). Mice with a fasting blood glucose level of ≥250 mg/dL for two consecutive measurements were classified as diabetic. Experiments were performed on female mice between P1 and 50 weeks of age.

Cell lines—INS1 832/3 cells[69] were maintained in RPMI 1640 medium supplemented with 10% calf serum, 10mM HEPES, 1mM Na-pyruvate, 2mM Glutamax, 1% antibiotic/antimycotic, and 50μM 2-mercaptoethanol. They were kept in a 37°C incubator with a humidified atmosphere of 5% CO_2 in air. Cells were used at passages between 25–40. NIT1 cells were purchased from ATCC (#CRL-2055). They were maintained in high-glucose DMEM medium supplemented with 10% FBS, 20mM HEPES, 1mM Na-pyruvate, 1X antibiotic/antimycotic, and 50μM 2-mercaptoethanol. They were kept in 37°C incubator with a humidified atmosphere of 5% CO_2 in air. Cells were used at passages between 20–35.

The human pancreatic β-cell line EndoC-βH1 was provided by R. Scharfmann (Institut Cochin, Université Paris, Paris, France).[70] The EndoC-βH1 cells were cultured in Dulbecco's modified Eagle medium with 5.6mM glucose, 2% fatty acid–free BSA fraction V, 50μM 2-mercaptoethanol, 10mM nicotinamide, 5.5μg/mL transferrin, 6.7ng/mL selenite, and 100U/ml penicillin + 100μg/mL streptomycin in Matrigel-fibronectin–coated plates.[7] All the experiments performed with cell lines refer to independent experiments.

Human islets—Human islets were procured through the Integrated Islet Distribution Program (IIDP) under the study, BS480P. Detailed information for donor islets used in this study is listed in Supplementary Table S2. Following receival, islets were cultured in complete PIM(S) (Prodo Labs) overnight at 37°C incubator with a humidified atmosphere of 5% CO_2 in air for recovery. The next day, they were treated with vehicle (DMSO), 0.25μg/mL tunicamycin, 15μM Ceapin-A7, and 50μM 4μ8C. After 48 hours, media of islets

were changed to fresh, serum-free, PIM(S) containing freshly added drugs. After 24 hours of incubation, conditioned media was collected, filtered, snap-frozen, and stored at −80°C. Islets were processed for RNA isolation using RNeasy Mini Kit (Qiagen). Equal amounts of RNA were used to synthesize cDNA (Thermo Fisher Scientific, #4368814). Quantitative RT-PCR was performed as described. Primers used to detect target genes are listed in Table S4.

Plasmids, AAV viruses, and reagents—3XFlag-CA-Atf6 was cloned to encode 1–360aa of mouse *Atf6* gene. 3Xflag tag was expressed at the N-terminal of the protein. CMV-GFP plasmid was a kind gift from Dr. Judith Simcox, UW-Madison. AAV8 viruses encoding for shRNA against mouse *Cdkn1a* with GFP tag under the control of rat *Ins1* promoter (Ramzy et al., 2020), as well as shScramble with GFP tag under the control of CMV promoter, were purchased from VectorBuilder. shRNA sequence against mouse *Cdkn1a* was: 5'AAGTTAGGACTCAACCGTAATATAGTGAAGCCACAGATGTATATTACGGTTGAGT CCTAACTG-3'.

The reagents used in the study were: tunicamycin (Sigma, #T7765), Ceapin-A7 (Sigma, #SML2330), forskolin (Cayman, #11018), p21 inhibitor; UC2288 (Sigma, #532813), CREB inhibitor; 666–15 (MedChem, #HY-101120), 4μ8C (Sigma, #SML0949), mouse LIF antibody (R&D systems, #AF449), and normal goat IgG control (R&D systems, #AB-108-C).

In vivo administration of virus and antibodies—1×10^{12} VG AAV8 viruses (encoding for sh*Cdkn1a* or shScramble) were injected intraperitoneally once to 3-week-old, female, Ire1α$^{\beta-/-}$ mice. At 5 weeks of age, pancreas tissue was extracted for histology and step-sections were obtained. 10μg mouse anti-LIF neutralizing antibody or 10μg normal goat IgG control were injected intraperitoneally into female Ire1α$^{\beta-/-}$ or Atf6$^{\beta-/-}$ mice every other day starting from 3-week-old until they reached 5-week-old.[71] At 5 weeks of age, pancreata were extracted for histological analyses.

Histology and immunofluorescence—Mice were euthanized, their pancreas removed and fixed in zinc formalin (Thermo Fisher Scientific). Paraffin-embedded pancreata were cut at 5μm thickness at 3 depths and 200μm between depths. One section at each depth was stained with H&E. Insulitis was scored as previously described.[13] "Peri-insulitis" is defined as focal aggregation at one pole of the islet and in contact with the islet periphery. "Non-aggressive insulitis" refers to lesions with clear, and often extensive, islet infiltrates occupying less than 50% of the islet area, whereas "aggressive insulitis" refers to an extensive infiltrate, where lymphoid cells invade the entire islet and intermingle with endocrine cells, showing extensive signs of β-cell damage.

For immunostaining, sodium citrate buffer pH6.0 at 95°C was used as antigen retrieval buffer. Anti-Insulin (Linco), anti-Glucagon (Cell Signaling, #2760S), anti-ATF6α (Santa Cruz, #sc22799), anti-Ki67 (Abcam, ab16667), anti-p21 (Abcam, ab188224), anti-pH2AX (Cell Signaling, #9718), anti-Arginase1 (Cell Signaling, #93668S), anti-GFP (Santa Cruz, sc#9996), Alexa Fluor 488 (Invitrogen, #A11073), and Alexa Fluor 568 (Invitrogen, #A11036) were used following established protocols. Sections were mounted using

mounting media containing 4′,6-diamidino-2-phenylindole dihydrochloride (DAPI) (Vector Labs, H-1800).

Microscopy—For islet morphometry measurements, images of the H&E-stained pancreatic sections were taken using an Amscope light microscope. The images of the immunostaining on pancreatic sections were obtained using a Nikon A1R-SI+ confocal microscope and a Nikon Storm/Tirf/Epifluorescence. The images were analyzed using Fiji image analysis software[72] and Nikon NIS-Elements by two experimenters blind to the genotypes.

Immunophenotyping—Prior to organ dissection, mice were perfused with 20mL PBS to eliminate contaminating blood leukocytes. Single-cell suspensions of the pancreata were prepared by Collagenase P (Roche) digestion. Cells from pancreatic lymph nodes and spleen were prepared by physical dissociation. All stainings began with incubation with TruStain fcX anti-mouse CD16/32. Antibodies used for subsequent stainings were anti-CD45 (30-F11), -CD19 (6D5); -CD3 (145–2C11), -CD4 (RM4–5), -CD8 (53–6.7), -CD25 (PC61), CD11b (M1/70), -CD11c (N418), -CD206 (C068C2), -F4/80 (BM8), and -Gr1 (RB6–8C5) (all from BioLegend). Intracellular Foxp3 (FJK-16s) staining was performed according to eBioscience's protocol. For M1/M2 macrophage analysis, pregated $CD45^+$ and $F4/80^+$ cells that were $CD11c^+/CD206^-$ were counted as M1, while $CD206^+/CD11c^-$ were counted as M2. Samples were acquired with an Attune NxT flow cytometer (Thermo Fisher Scientific) or LSRFortessa X-20 (BD Biosciences), and data were analyzed with FlowJo software (Tree Star, Inc.).

Islet isolation—Islets were isolated by using the standard collagenase/protease digestion method. Briefly, the pancreatic duct was cannulated and distended with 4°C 0.5mg/mL collagenase/protease solution using Collagenase P (Sigma-Aldrich). The reaction was stopped using 10% fetal bovine serum in RPMI 1640 (Gibco) before being washed three times with a 0.02% bovine serum albumin solution (Sigma Aldrich) in 1X Hank's balanced solution (Corning). The islets were separated from the exocrine tissue by using a gradient of Histopaque-1077 (Sigma-Aldrich) and serum-free RPMI 1640 [73]. Islets were hand-picked and cultured overnight at 37°C prior to the experiments.

C_{12}FDG staining and cell size analyses—Analysis of SA-β-gal activity by C_{12}FDG staining was performed according to a previously published method[74] with some modifications. Briefly, isolated islets were dispersed using Accutase (Innovative Cell Technologies, #AT104) and pre-strained using a 40μm filter. Dispersed islet cells were incubated with 33μM C_{12}FDG (Cayman Chemical, #25583) for 1 hour at 37°C before being washed twice with cell staining buffer (Biolegend, #420201) and incubated with TruStain fcX anti-mouse CD16/32 (Biolegend, #101319) for 10 minutes. Immune cells were able to be excluded from our analyses with staining of anti-CD45 (Biolegend, #103133). Prior to analyses, cells were incubated with propidium iodide (PI) for 15 minutes. Cells were gated for debris exclusion (FSC-A/SSC-A), singlets (FSC-H/FSC-A), viability (PI^-), and non-immune cells ($CD45^-$). Cells were analyzed for forward scatter (FSC-A) for the size

analyses, and C_{12}FDG fluorescence for the SA-βGAL analyses. Samples were run using a LSRFortessa X-20 (BD Biosciences) and analyzed with FlowJo software (Tree Star, Inc.).

Apoptosis assay—Dispersed islet cells were filtered using a 40μm mesh and washed with Annexin V binding buffer (Biolegend, #422201). After filtration, cells were incubated with FITC-conjugated Annexin V and propidium iodide (Biolegend, #640914). Cells were gated for debris exclusion (FSC-A/SSC-A) and singlets (FSC-H/FSC-A). Cells that were positive for Annexin V and PI were considered as apoptotic. Samples were run using a LSRFortessa X-20 (BD Biosciences) and analyzed with FlowJo software (Tree Star, Inc.).

Cell cycle analysis—Following dispersion, islet cells were washed twice with phosphate-buffered saline (PBS). After the second wash, supernatant was removed until 1mL of PBS remains. While vortexing gently at the lowest speed, 4mL of 100% ethanol was slowly added dropwise to the sample for fixation overnight. After fixation, cells were rehydrated with PBS for 15 minutes and then incubated with 3μg/mL DAPI solution (Biolegend, #422801) overnight at 4°C. Cells were gated for debris exclusion (FSC-A/SSC-A) and singlets (FSC-H/FSC-A) prior to cell cycle analysis. Samples were run with a LSRFortessa X-20 (BD Biosciences) and analyzed with FlowJo software (Tree Star, Inc.).

ELISA—Serum insulin levels of mice were quantified by ELISA (n=4–5) at 13 weeks of age according to manufacturer's instructions (Alpco, Ultrasensitive Mouse Insulin ELISA). Mouse CXCL14 levels were determined by according to manufacturer's instructions (RayBiotech, ELM-CXCL14).

RNA isolation and quantitative-PCR—Samples from cell lines and mouse islets were collected with TRIzol reagent (Invitrogen, #15596026) and RNA isolation was performed following the product manual. Turbo DNase kit (Invitrogen, #AM1907) was used following manufacturer's protocol to remove genomic DNA. Equal amounts of RNA were used to synthesize cDNA (Thermo Fisher Scientific, #4368814). Quantitative PCR (qPCR) was done using Power SYBR Green master mix (Applied Biosystems, #4368708). Primers used to detect target genes are listed in Table S4.

Western blotting—INS1 832/3 or NIT1 cells were collected with cold RIPA buffer (0.1% SDS, 1mM EDTA, 50mM Tris-HCl, pH7.5, 150mM NaCl, 1% Triton X-100 supplemented with 30mM NaF, 10mM Na_3VO_4, 1mM PMSF, and 1X protease inhibitor cocktail (Sigma, #8340). Samples were briefly sonicated with Branson sonicator to pellet genomic DNA. Samples were centrifuged at 14000rpm for 15 minutes at 4°C and supernatant transferred into new tubes. Protein concentrations were measured with BCA assay (Thermo Fisher Scientific, #23227). Equal amounts of protein (25–30μg) were loaded for each sample. Samples were resolved in 10% SDS-PAGE gel. Following wet transfer to PVDF membranes and 1 hour of blocking with 5% nonfat-dry milk in TBS-T, membranes left to incubate with primary antibodies in blocking buffer (anti-p21, 1:200, sc#53870; anti-NRF2, 1:500, CST#12721; anti-cleaved caspase 3, 1:500, CST#9661; anti-phospho CREB, 1:200, sc#81486; anti-CREB, 1:1000, Millipore#06–863; anti-β-actin, 1:5000, sc#47778) overnight at 4°C. The next day, membranes were washed with TBS-T and incubated with appropriate HRP conjugated secondary antibodies in blocking buffer (anti-rabbit, 1:2000,

CST#7074; anti-mouse, 1:2000, CST#7076) for 2 hours at room temperature. Membranes were developed with SuperSignal West Pico Plus (Thermo Fisher Scientific, #34577) and imaged with Azure Imaging Systems. Quantification of bands was done following background corrections using Image Studio Lite Ver 5.2.

EMSA—6μg nuclear lysate was incubated with 75fmol radiolabeled DNA substrates in 50mM Tris-HCl (pH8.0), 0.1mg/mL bovine serum albumin, 2mM dithiothreitol, 5mM ethylenediaminetetraacetic acid, 1μg/mL poly dI-dC, and 6% glycerol at room temperature for 30 minutes. Where indicated, unlabeled DNA competitors were included at 10X or 25X molar excess of the radiolabeled DNA substrate. The samples were resolved through a 6% TBE-PAGE gel (6% Acryl/Bis 29:1, 0.5X TBE) for three hours at 80V. Gels were dried with a vacuum gel-dryer for one hour at 80°C. Dried gels were exposed to Storage Phospho screens overnight and imaged with a Typhoon FLA 9500. Images were quantified using ImageQuant software. Assay was repeated with nuclear lysates collected 3 independent times.

Chromatin Immunoprecipitation assay followed by quantitative PCR—Chromatin immunoprecipitation was performed as described previously with the following adjustments (Bayam et al., 2015). INS1 832/3 cells were fixed with 1% formaldehyde for 10 minutes following quenching with 125mM glycine for 10 minutes at room temperature with slow shaking. Cells were collected with ChIP Lysis buffer: 1% SDS, 10mM EDTA, 50mM Tris-HCl, pH8.0 supplemented with 30mM NaF, 10mM Na_3VO_4, 1mM PMSF, and 1X protease inhibitor cocktail (Sigma, #8340). Cell lysates were sonicated using with Branson sonicator to obtain DNA fragments around 500bp. They were centrifuged at 14000rpm for 20 minutes to collect supernatant and diluted at 1:4 ratio with 1% Triton X-100, 2mM EDTA, 20mM Tris-HCl pH8.0, 150mM NaCl, supplemented with 30mM NaF, 10mM Na_3VO_4, 1mM PMSF, and 1X protease inhibitor cocktail. Samples were pre-cleared for an hour with Protein A+Protein G magnetic beads at 4°C on a rotator. 1% of the sample was reserved for input control. Chromatin was immunoprecipitated with 1ug p-CREB (Millipore #06–519), 1μg sXBP1 (Cell Signaling, #82914) or 1μg IgG (Cell Signaling, #3900) antibodies at 4°C overnight on a rotator. The next day, protein-antibody complexes were captured onto Protein A+Protein G magnetic beads and the beads were washed twice with High Salt wash buffer (500mM NaCl, 1% Triton X-100, 20mM Tris-HCl, pH 8.0, 0.1% SDS and 2mM EDTA), Low Salt wash buffer (150mM NaCl, 1% Triton X-100, 20mM Tris-HCl, pH 8.0, 0.1% SDS and 2mM EDTA) and LiCl wash buffer (250mM LiCl, 1% Na-DOC, 10mM Tris-HCl, pH8.0, 1% NP-40 and 1mM EDTA). DNA complexes were eluted from the beads with 1% SDS and 100mM $NaHCO_3$ at 65°C for an hour. Following removal of beads, the immunoprecipitated samples as well as input sample were left at 65°C overnight for reverse-crosslinking. The next day, equal volumes of 100mM Tris-HCl, pH 8.0 and 20mM EDTA were added to samples. Following 1 hour of RNase A (Thermo Fisher Scientific, #EN0531) incubation at 37°C and 2 hours of Proteinase K (Thermo Fisher Scientific, #EO0491) incubation at 50°C, eluted DNA samples were purified with phenol-chloroform extraction. DNA pellets were reconstituted in 30μl nuclease-free water. For qPCR, equal volume of samples was used to amplify target regions.

Following PCR primers used for qPCR; *Hspa5* F: 5'- GGTGGCATGAACCAACCAG-3', R: 5'GCTTATATATCCTCCCCGC-3', *p21* F: 5'- GGCTCATCGTGACGTGTTT-3', R: 5'- CAAGGAGTGGTGAGTCAGTTTC-3', *p21 3' UTR* F: 5'- GAAGGGAACGGGTACACAGG-3', R: 5'- ACACACACAGGGATGCTCTG-3'. The numerical value 6.64 ($\log_2(0.01)$, representing 1% of input chromatin) was subtracted from the Ct value of the input sample to generate the adjusted input Ct. The following formula was used to calculate the % input normalized ChIP'ed DNA amount: $100 \times 2^{(\text{Adjusted input Ct} - \text{ChIP Ct})}$.

Transfection and nuclear extraction—INS1 832/3 cells were reverse transfected using Lipofectamine 2000 (Invitrogen, #11668027). At the day of transfection, cells were trypsinized, counted and 2 million cells were seeded to one-well of 6-well plate. Empty backbone vector (p3X-Flag-CMV.10, Sigma), GFP, and 3XFlag-CA-Atf6 vectors were prepared with Lipofectamine 2000 at 1:4 ratio. Transfection was done using manufacturer's protocol. After 18 hours of transfection, cells were treated with either vehicle (DMSO) or 20μM forskolin. After 6 hours of treatment, cells were collected and nuclear extraction was performed using nuclear extraction kit (Cayman, #10009277). Nuclear lysates were aliquoted, snap-frozen and stored at −80°C until further use.

Conditioned media collection—NIT1 cells were seeded in 6-well plates a day before treatments. Cells were treated with vehicle (DMSO), 6μM Ceapin-A7, and 2.5μM p21 inhibitor (UC2288) as indicated. After 48 hours, whole media of cells were replaced with fresh media containing treatments. After 24 hours, the media with drugs were removed from cells and media containing 5% FBS without any drugs were added to collect conditioned media (CM). 24 hours later, CM was collected, filtered with 0.2μm filter and stored at 4°C. For LIF neutralization experiment, CM was treated with either 1μg IgG or anti-LIF antibody for 3 hours to allow the anti-LIF antibodies to bind. Then, the actual migration assay was done over 48 hours. All collected CM were used within 3 weeks of collection for transwell migration assays.

Isolation of peritoneal immune cells—4- to 6-week-old male NOD mice were used to collect the peritoneal immune cells using 4mL of ice-cold PBS supplemented with 3% FBS as described previously.[75] The immune cells were centrifuged at 1500rpm for 8 min at 4°C. Cells were counted and subjected to transwell migration assays.

Transwell migration assay—To perform transwell migration assays using peritoneal immune cells, 500μl of CM was added to a 24-well plate with coverslip. A transwell insert (3μm pore size, Costar, #3415) was loaded with ~2.8×10^5 peritoneal immune cells in 100μl of medium (matching the medium used for CM production). Immune cells were allowed to migrate for 42 hours. Migrated lymphocytes (suspension cells) were counted using hematocytometer. Migrated adherent cells (macrophages) at the insert membrane were counted either after crystal violet staining on the membrane itself or on the glass coverslips after imaging with bright-field microscope. For crystal violet staining, membranes were stained as described previously.[76]

Staining and sorting β-cells for RNA-seq—Following isolation of islets from 6-week-old mice, islets were dispersed into single cells and β-cells were sorted for RNA-seq as previously described.[25] Briefly, isolated islets were dispersed and stained with Ghost Dye Red 780 (Tonbo Biosciences) and anti-CD45 (BD Biosciences) antibodies. Next, cells were fixed with 4% paraformaldehyde (Electron Microscopy Sciences) and permeabilized with 0.1% saponin (Sigma-Aldrich) according to manufacturer's instructions before being stained with anti-insulin (R&D Systems) and anti-glucagon (BD Biosciences) antibodies. B-cells were then sorted by using FACSAria II (BD Biosciences).

Bulk RNA-seq—Following sorting, fixed β-cells were processed using the RecoverAll Total Nucleic Acid Isolation kit (Ambion) until the protease digestion stage. Then, RNA was extracted using the RNeasy Micro Kit (Qiagen) including a column for elimination of genomic DNA. RNA concentration was determined using 2100 Bioanalyzer instrument (Agilent Technologies). RNA Integrity Number (RIN) was measured using Agilent RNA 6000 Pico Kit (Agilent Technologies). The RNA integrity number (RIN) of samples ranged from 7.8 to 9.8. RIN > 8 was used in the experiments. RNA library is generated using the TruSeq Stranded Total RNA (Human/Mouse/Rat) (Illumina Inc). Cytoplasmic ribosomal RNA is removed from the sample using complementary probe sequences attached to magnetic beads. Subsequently, each mRNA sample is fragmented using divalent cations under elevated temperature and purified. First-strand cDNA synthesis is performed using SuperScriptII Reverse Transcriptase (Invitrogen) and random primers. Second strand cDNAs are synthesized using DNA Polymerase I and RNase H for removal of mRNA. Double-stranded cDNA is purified using Agencourt AMPure XP beads (Qiagen) as recommended in the TruSeq RNA Sample Prep Guide. The blunt ended cDNA and the adapter-ligated products are purified using Agencourt AMPure XP beads. Quality and quantity of finished libraries are assessed using an Agilent DNA1000 series chip assay (Agilent Technologies) and Invitrogen Qubit HS cDNA Kit (Invitrogen), respectively. Cluster generation is performed using a TruSeq Paired End Cluster Kit (v4) and the Illumina cBot, with libraries multiplexed for 1×100bp sequencing using the TruSeq 250bp SBS kit (v4) on an Illumina HiSeq2500.

Single-cell RNA sequencing and differential gene expression (DGE) analysis —Generation of single cell RNA sequencing data for Ire1α$^{\beta-/-}$ mice was previously described.[13] DGE analysis was performed by using Monocle v2.8.0.[77]

Single-cell RNA sequencing analysis from human donors—scRNA-seq analysis on β-cells from T1D and healthy human donors have been performed as described previously.[68] Briefly, the scRNA-seq raw data from T1D and healthy donors' datasets were obtained from HPAP (https://hpap.pmacs.upenn.edu/).[44] The raw data pooled and normalized using SCtransform in the Seurat package in R. Cell types were assigned by Seurat clustering results according to the expression of pancreatic marker genes.[78] Non-supervised Uniform Manifold Approximation and Projection (UMAP) of the dataset to cluster cells with similar expression profiles have been applied.

QUANTIFICATION AND STATISTICAL ANALYSIS

For all experiments, the statistical analyses, error bars, and number of biological replicates are described in the figure legends. A minimum of n = 3 or more biological replicates were used for all statistical analyses. Sample sizes were based on pilot experiments and previously published work.[9,13] For quantification of IF images and insulitis scoring, each sample was blinded for data analysis to prevent bias. Data are represented as mean ± SEM and were represented and analyzed in GraphPad Prism (GraphPad Software).

Supplementary Material

Refer to Web version on PubMed Central for supplementary material.

ACKLNOWLEDGEMENTS

We thank Quincy Harenda and Muhyiddin Bera Demirtas for their technical assistance. Graphical abstract and cartoons were created using BioRender.com. H.L. was supported by the T32 GM007215 and a UW-SCRMC Graduate Fellowship. Human islets were provided by the Integrated Islet Distribution Program-Islet Award Initiative. P.J.T. was supported by grants from the University of Manitoba (URGP), the Children's Hospital Research Institute of Manitoba (CHRIM OG-2021-05) and the Canadian Institutes of Health Research (CIHR PJT-479641). M.H. was supported by the NIH (DK053307 and DK060596). D.L.E. was supported by grants from the Welbio-FNRS (WELBIO-CR-2019C-04), the Dutch Diabetes Research Foundation (Innovate2CureType1), the JDRF (3-SRA-2022-1201-S-B); the NIH-HIRN-CBDS (U01 DK127786); the NIH (DK126444 and DK133881-01); and the Innovative Medicines Initiative 2 Joint Undertaking under grant agreements 115797 (INNODIA) and 945268 (INNODIA HARVEST), receiving support from the European Union's Horizon 2020 research and innovation program and "EFPIA", "JDRF" and "The Leona M. and Harry B. Helmsley Charitable Trust" F.E. is supported by grants from the NIH (DK130919 and DK128136), JDRF (3-SRA-2023-1315-S-B and 5-CDA-2014-184-A-N), Greater Milwaukee Foundation, and startup funds from the UW-Madison.

REFERENCES

1. Harding HP, Zhang Y, Zeng H, Novoa I, Lu PD, Calfon M, Sadri N, Yun C, Popko B, Paules R, et al. (2003). An integrated stress response regulates amino acid metabolism and resistance to oxidative stress. Mol Cell 11, 619–633. 10.1016/s1097-2765(03)00105-9. [PubMed: 12667446]
2. Bernales S, Papa FR, and Walter P (2006). Intracellular signaling by the unfolded protein response. Annu Rev Cell Dev Biol 22, 487–508. 10.1146/annurev.cellbio.21.122303.120200. [PubMed: 16822172]
3. Walter P, and Ron D (2011). The unfolded protein response: from stress pathway to homeostatic regulation. Science 334, 1081–1086. 10.1126/science.1209038. [PubMed: 22116877]
4. Engin F (2016). ER stress and development of type 1 diabetes. J Investig Med 64, 2–6. 10.1097/JIM.0000000000000229.
5. Eizirik DL, Pasquali L, and Cnop M (2020). Pancreatic beta-cells in type 1 and type 2 diabetes mellitus: different pathways to failure. Nat Rev Endocrinol 16, 349–362. 10.1038/s41574-020-0355-7. [PubMed: 32398822]
6. Cefalu WT, Andersen DK, Arreaza-Rubin G, Pin CL, Sato S, Verchere CB, Woo M, Rosenblum ND, Symposium planning committee, m., speakers, et al. (2021). Heterogeneity of Diabetes: beta-Cells, Phenotypes, and Precision Medicine: Proceedings of an International Symposium of the Canadian Institutes of Health Research's Institute of Nutrition, Metabolism and Diabetes and the U.S. National Institutes of Health's National Institute of Diabetes and Digestive and Kidney Diseases. Diabetes. 10.2337/db21-0777.
7. Brozzi F, Nardelli TR, Lopes M, Millard I, Barthson J, Igoillo-Esteve M, Grieco FA, Villate O, Oliveira JM, Casimir M, et al. (2015). Cytokines induce endoplasmic reticulum stress in human, rat and mouse beta cells via different mechanisms. Diabetologia 58, 2307–2316. 10.1007/s00125-015-3669-6. [PubMed: 26099855]

8. Cardozo AK, Ortis F, Storling J, Feng YM, Rasschaert J, Tonnesen M, Van Eylen F, Mandrup-Poulsen T, Herchuelz A, and Eizirik DL (2005). Cytokines downregulate the sarcoendoplasmic reticulum pump Ca2+ ATPase 2b and deplete endoplasmic reticulum Ca2+, leading to induction of endoplasmic reticulum stress in pancreatic beta-cells. Diabetes 54, 452–461. 10.2337/diabetes.54.2.452. [PubMed: 15677503]
9. Engin F, Yermalovich A, Nguyen T, Hummasti S, Fu W, Eizirik DL, Mathis D, and Hotamisligil GS (2013). Restoration of the unfolded protein response in pancreatic beta cells protects mice against type 1 diabetes. Sci Transl Med 5, 211ra156. 10.1126/scitranslmed.3006534.
10. Evans-Molina C, Sims EK, DiMeglio LA, Ismail HM, Steck AK, Palmer JP, Krischer JP, Geyer S, Xu P, Sosenko JM, and Type 1 Diabetes TrialNet Study, G. (2018). beta Cell dysfunction exists more than 5 years before type 1 diabetes diagnosis. JCI Insight 3. 10.1172/jci.insight.120877.
11. Sims EK, Mirmira RG, and Evans-Molina C (2020). The role of beta-cell dysfunction in early type 1 diabetes. Curr Opin Endocrinol Diabetes Obes 27, 215–224. 10.1097/MED.0000000000000548. [PubMed: 32618633]
12. Tersey SA, Nishiki Y, Templin AT, Cabrera SM, Stull ND, Colvin SC, Evans-Molina C, Rickus JL, Maier B, and Mirmira RG (2012). Islet beta-cell endoplasmic reticulum stress precedes the onset of type 1 diabetes in the nonobese diabetic mouse model. Diabetes 61, 818–827. 10.2337/db11-1293. [PubMed: 22442300]
13. Lee H, Lee YS, Harenda Q, Pietrzak S, Oktay HZ, Schreiber S, Liao Y, Sonthalia S, Ciecko AE, Chen YG, et al. (2020). Beta Cell Dedifferentiation Induced by IRE1alpha Deletion Prevents Type 1 Diabetes. Cell Metab 31, 822–836 e825. 10.1016/j.cmet.2020.03.002. [PubMed: 32220307]
14. Morita S, Villalta SA, Feldman HC, Register AC, Rosenthal W, Hoffmann-Petersen IT, Mehdizadeh M, Ghosh R, Wang L, Colon-Negron K, et al. (2017). Targeting ABL-IRE1alpha Signaling Spares ER-Stressed Pancreatic beta Cells to Reverse Autoimmune Diabetes. Cell Metab 25, 883–897 e888. 10.1016/j.cmet.2017.03.018. [PubMed: 28380378]
15. Sahin GS, Lee H, and Engin F (2021). An accomplice more than a mere victim: The impact of beta-cell ER stress on type 1 diabetes pathogenesis. Mol Metab 54, 101365. 10.1016/j.molmet.2021.101365. [PubMed: 34728341]
16. Gasek NS, Kuchel GA, Kirkland JL, and Xu M (2021). Strategies for Targeting Senescent Cells in Human Disease. Nat Aging 1, 870–879. 10.1038/s43587-021-00121-8. [PubMed: 34841261]
17. Di Micco R, Krizhanovsky V, Baker D, and d'Adda di Fagagna F (2021). Cellular senescence in ageing: from mechanisms to therapeutic opportunities. Nat Rev Mol Cell Biol 22, 75–95. 10.1038/s41580-020-00314-w. [PubMed: 33328614]
18. Kang TW, Yevsa T, Woller N, Hoenicke L, Wuestefeld T, Dauch D, Hohmeyer A, Gereke M, Rudalska R, Potapova A, et al. (2011). Senescence surveillance of pre-malignant hepatocytes limits liver cancer development. Nature 479, 547–551. 10.1038/nature10599. [PubMed: 22080947]
19. Ovadya Y, Landsberger T, Leins H, Vadai E, Gal H, Biran A, Yosef R, Sagiv A, Agrawal A, Shapira A, et al. (2018). Impaired immune surveillance accelerates accumulation of senescent cells and aging. Nat Commun 9, 5435. 10.1038/s41467-018-07825-3. [PubMed: 30575733]
20. Sturmlechner I, Zhang C, Sine CC, van Deursen EJ, Jeganathan KB, Hamada N, Grasic J, Friedman D, Stutchman JT, Can I, et al. (2021). p21 produces a bioactive secretome that places stressed cells under immunosurveillance. Science 374, eabb3420. 10.1126/science.abb3420. [PubMed: 34709885]
21. Yousefzadeh MJ, Flores RR, Zhu Y, Schmiechen ZC, Brooks RW, Trussoni CE, Cui Y, Angelini L, Lee KA, McGowan SJ, et al. (2021). An aged immune system drives senescence and ageing of solid organs. Nature 594, 100–105. 10.1038/s41586-021-03547-7. [PubMed: 33981041]
22. Thompson PJ, Shah A, Ntranos V, Van Gool F, Atkinson M, and Bhushan A (2019). Targeted Elimination of Senescent Beta Cells Prevents Type 1 Diabetes. Cell Metab 29, 1045–1060 e1010. 10.1016/j.cmet.2019.01.021. [PubMed: 30799288]
23. Yamamoto K, Sato T, Matsui T, Sato M, Okada T, Yoshida H, Harada A, and Mori K (2007). Transcriptional Induction of Mammalian ER Quality Control Proteins Is Mediated by Single or Combined Action of ATF6α and XBP1. Developmental Cell 13, 365–376. 10.1016/j.devcel.2007.07.018. [PubMed: 17765680]

24. Sharma RB, O'Donnell AC, Stamateris RE, Ha B, McCloskey KM, Reynolds PR, Arvan P, and Alonso LC (2015). Insulin demand regulates beta cell number via the unfolded protein response. J Clin Invest 125, 3831–3846. 10.1172/JCI79264. [PubMed: 26389675]
25. Hrvatin S, Deng F, O'Donnell CW, Gifford DK, and Melton DA (2014). MARIS: method for analyzing RNA following intracellular sorting. PLoS One 9, e89459. 10.1371/journal.pone.0089459. [PubMed: 24594682]
26. Williams AB, and Schumacher B (2016). p53 in the DNA-Damage-Repair Process. Cold Spring Harbor Perspectives in Medicine 6. 10.1101/cshperspect.a026070.
27. Brawerman G, Pipella J, and Thompson PJ (2022). DNA damage to beta cells in culture recapitulates features of senescent beta cells that accumulate in type 1 diabetes. Mol Metab 62, 101524. 10.1016/j.molmet.2022.101524. [PubMed: 35660116]
28. Mah LJ, El-Osta A, and Karagiannis TC (2010). gammaH2AX: a sensitive molecular marker of DNA damage and repair. Leukemia 24, 679–686. 10.1038/leu.2010.6. [PubMed: 20130602]
29. Walker EM, Cha J, Tong X, Guo M, Liu JH, Yu S, Iacovazzo D, Mauvais-Jarvis F, Flanagan SE, Korbonits M, et al. (2021). Sex-biased islet beta cell dysfunction is caused by the MODY MAFA S64F variant by inducing premature aging and senescence in males. Cell Rep 37, 109813. 10.1016/j.celrep.2021.109813. [PubMed: 34644565]
30. Jiang Z, Li H, Schroer SA, Voisin V, Ju Y, Pacal M, Erdmann N, Shi W, Chung PED, Deng T, et al. (2022). Hypophosphorylated pRb knock-in mice exhibit hallmarks of aging and vitamin C-preventable diabetes. EMBO J 41, e106825. 10.15252/embj.2020106825. [PubMed: 35023164]
31. Wettersten HI, Hee Hwang S, Li C, Shiu EY, Wecksler AT, Hammock BD, and Weiss RH (2013). A novel p21 attenuator which is structurally related to sorafenib. Cancer Biol Ther 14, 278–285. 10.4161/cbt.23374. [PubMed: 23298903]
32. Yang J, Zhang W, Jiang W, Sun X, Han Y, Ding M, Shi Y, and Deng H (2009). P21cip-overexpression in the mouse beta cells leads to the improved recovery from streptozotocin-induced diabetes. PLoS One 4, e8344. 10.1371/journal.pone.0008344. [PubMed: 20020058]
33. Sassone-Corsi P, Visvader J, Ferland L, Mellon PL, and Verma IM (1988). Induction of proto-oncogene fos transcription through the adenylate cyclase pathway: characterization of a cAMP-responsive element. Genes Dev 2, 1529–1538. 10.1101/gad.2.12a.1529. [PubMed: 2850967]
34. Wang Y, Vera L, Fischer WH, and Montminy M (2009). The CREB coactivator CRTC2 links hepatic ER stress and fasting gluconeogenesis. Nature 460, 534–537. 10.1038/nature08111. [PubMed: 19543265]
35. Gallagher CM, Garri C, Cain EL, Ang KK, Wilson CG, Chen S, Hearn BR, Jaishankar P, Aranda-Diaz A, Arkin MR, et al. (2016). Ceapins are a new class of unfolded protein response inhibitors, selectively targeting the ATF6alpha branch. Elife 5. 10.7554/eLife.11878.
36. Xie F, Li BX, Kassenbrock A, Xue C, Wang X, Qian DZ, Sears RC, and Xiao X (2015). Identification of a Potent Inhibitor of CREB-Mediated Gene Transcription with Efficacious in Vivo Anticancer Activity. J Med Chem 58, 5075–5087. 10.1021/acs.jmedchem.5b00468. [PubMed: 26023867]
37. Shin S, Le Lay J, Everett LJ, Gupta R, Rafiq K, and Kaestner KH (2014). CREB mediates the insulinotropic and anti-apoptotic effects of GLP-1 signaling in adult mouse beta-cells. Mol Metab 3, 803–812. 10.1016/j.molmet.2014.08.001. [PubMed: 25379405]
38. Zhang C, Yu Y, Ma L, and Fu P (2020). Histamine H3 Receptor Promotes Cell Survival via Regulating PKA/CREB/CDKN1A Signal Pathway in Hepatocellular Carcinoma. Onco Targets Ther 13, 3765–3776. 10.2147/OTT.S250655. [PubMed: 32440145]
39. Yoshida H, Matsui T, Yamamoto A, Okada T, and Mori K (2001). XBP1 mRNA is induced by ATF6 and spliced by IRE1 in response to ER stress to produce a highly active transcription factor. Cell 107, 881–891. [PubMed: 11779464]
40. Carrero JA, Ferris ST, and Unanue ER (2016). Macrophages and dendritic cells in islets of Langerhans in diabetic autoimmunity: a lesson on cell interactions in a mini-organ. Curr Opin Immunol 43, 54–59. 10.1016/j.coi.2016.09.004. [PubMed: 27710840]
41. Stempin CC, Dulgerian LR, Garrido VV, and Cerban FM (2010). Arginase in parasitic infections: macrophage activation, immunosuppression, and intracellular signals. J Biomed Biotechnol 2010, 683485. 10.1155/2010/683485. [PubMed: 20029630]

42. Sugiura S, Lahav R, Han J, Kou SY, Banner LR, de Pablo F, and Patterson PH (2000). Leukaemia inhibitory factor is required for normal inflammatory responses to injury in the peripheral and central nervous systems in vivo and is chemotactic for macrophages in vitro. Eur J Neurosci 12, 457–466. 10.1046/j.1460-9568.2000.00922.x. [PubMed: 10712626]
43. Hernandez-Segura A, Nehme J, and Demaria M (2018). Hallmarks of Cellular Senescence. Trends Cell Biol 28, 436–453. 10.1016/j.tcb.2018.02.001. [PubMed: 29477613]
44. Kaestner KH, Powers AC, Naji A, Consortium H, and Atkinson MA (2019). NIH Initiative to Improve Understanding of the Pancreas, Islet, and Autoimmunity in Type 1 Diabetes: The Human Pancreas Analysis Program (HPAP). Diabetes 68, 1394–1402. 10.2337/db19-0058. [PubMed: 31127054]
45. Fonseca SG, Ishigaki S, Oslowski CM, Lu S, Lipson KL, Ghosh R, Hayashi E, Ishihara H, Oka Y, Permutt MA, and Urano F (2010). Wolfram syndrome 1 gene negatively regulates ER stress signaling in rodent and human cells. J Clin Invest 120, 744–755. 10.1172/JCI39678. [PubMed: 20160352]
46. Teodoro T, Odisho T, Sidorova E, and Volchuk A (2012). Pancreatic beta-cells depend on basal expression of active ATF6alpha-p50 for cell survival even under nonstress conditions. Am J Physiol Cell Physiol 302, C992–1003. 10.1152/ajpcell.00160.2011. [PubMed: 22189555]
47. Dooley J, Tian L, Schonefeldt S, Delghingaro-Augusto V, Garcia-Perez JE, Pasciuto E, Di Marino D, Carr EJ, Oskolkov N, Lyssenko V, et al. (2016). Genetic predisposition for beta cell fragility underlies type 1 and type 2 diabetes. Nat Genet 48, 519–527. 10.1038/ng.3531. [PubMed: 26998692]
48. Kolb H, and Eizirik DL (2011). Resistance to type 2 diabetes mellitus: a matter of hormesis? Nat Rev Endocrinol 8, 183–192. 10.1038/nrendo.2011.158. [PubMed: 22024974]
49. Luchsinger LL (2021). Hormetic endoplasmic reticulum stress in hematopoietic stem cells. Curr Opin Hematol 28, 417–423. 10.1097/MOH.0000000000000668. [PubMed: 34232142]
50. Paramos-de-Carvalho D, Jacinto A, and Saude L (2021). The right time for senescence. Elife 10. 10.7554/eLife.72449.
51. Binet F, Cagnone G, Crespo-Garcia S, Hata M, Neault M, Dejda A, Wilson AM, Buscarlet M, Mawambo GT, Howard JP, et al. (2020). Neutrophil extracellular traps target senescent vasculature for tissue remodeling in retinopathy. Science 369. 10.1126/science.aay5356.
52. Da Silva-Alvarez S, Guerra-Varela J, Sobrido-Camean D, Quelle A, Barreiro-Iglesias A, Sanchez L, and Collado M (2020). Cell senescence contributes to tissue regeneration in zebrafish. Aging Cell 19, e13052. 10.1111/acel.13052. [PubMed: 31670873]
53. Krizhanovsky V, Yon M, Dickins RA, Hearn S, Simon J, Miething C, Yee H, Zender L, and Lowe SW (2008). Senescence of activated stellate cells limits liver fibrosis. Cell 134, 657–667. 10.1016/j.cell.2008.06.049. [PubMed: 18724938]
54. Meyer K, Hodwin B, Ramanujam D, Engelhardt S, and Sarikas A (2016). Essential Role for Premature Senescence of Myofibroblasts in Myocardial Fibrosis. J Am Coll Cardiol 67, 2018–2028. 10.1016/j.jacc.2016.02.047. [PubMed: 27126529]
55. Munoz-Espin D, and Serrano M (2014). Cellular senescence: from physiology to pathology. Nat Rev Mol Cell Biol 15, 482–496. 10.1038/nrm3823. [PubMed: 24954210]
56. Rhinn M, Ritschka B, and Keyes WM (2019). Cellular senescence in development, regeneration and disease. Development 146. 10.1242/dev.151837.
57. Ritschka B, Storer M, Mas A, Heinzmann F, Ortells MC, Morton JP, Sansom OJ, Zender L, and Keyes WM (2017). The senescence-associated secretory phenotype induces cellular plasticity and tissue regeneration. Genes Dev 31, 172–183. 10.1101/gad.290635.116. [PubMed: 28143833]
58. Sarig R, Rimmer R, Bassat E, Zhang L, Umansky KB, Lendengolts D, Perlmoter G, Yaniv K, and Tzahor E (2019). Transient p53-Mediated Regenerative Senescence in the Injured Heart. Circulation 139, 2491–2494. 10.1161/CIRCULATIONAHA.119.040125. [PubMed: 31107623]
59. Saul D, Monroe DG, Rowsey JL, Kosinsky RL, Vos SJ, Doolittle ML, Farr JN, and Khosla S (2021). Modulation of fracture healing by the transient accumulation of senescent cells. Elife 10. 10.7554/eLife.69958.

60. Parsa R, Andresen P, Gillett A, Mia S, Zhang XM, Mayans S, Holmberg D, and Harris RA (2012). Adoptive transfer of immunomodulatory M2 macrophages prevents type 1 diabetes in NOD mice. Diabetes 61, 2881–2892. 10.2337/db11-1635. [PubMed: 22745325]

61. Juhas U, Ryba-Stanislawowska M, Brandt-Varma A, Mysliwiec M, and Mysliwska J (2019). Monocytes of newly diagnosed juvenile DM1 patients are prone to differentiate into regulatory IL-10(+) M2 macrophages. Immunol Res 67, 58–69. 10.1007/s12026-019-09072-0. [PubMed: 30820875]

62. Egashira M, Hirota Y, Shimizu-Hirota R, Saito-Fujita T, Haraguchi H, Matsumoto L, Matsuo M, Hiraoka T, Tanaka T, Akaeda S, et al. (2017). F4/80+ Macrophages Contribute to Clearance of Senescent Cells in the Mouse Postpartum Uterus. Endocrinology 158, 2344–2353. 10.1210/en.2016-1886. [PubMed: 28525591]

63. Kale A, Sharma A, Stolzing A, Desprez PY, and Campisi J (2020). Role of immune cells in the removal of deleterious senescent cells. Immun Ageing 17, 16. 10.1186/s12979-020-00187-9. [PubMed: 32518575]

64. Prata L, Ovsyannikova IG, Tchkonia T, and Kirkland JL (2018). Senescent cell clearance by the immune system: Emerging therapeutic opportunities. Semin Immunol 40, 101275. 10.1016/j.smim.2019.04.003. [PubMed: 31088710]

65. Irvine KM, Skoien R, Bokil NJ, Melino M, Thomas GP, Loo D, Gabrielli B, Hill MM, Sweet MJ, Clouston AD, and Powell EE (2014). Senescent human hepatocytes express a unique secretory phenotype and promote macrophage migration. World J Gastroenterol 20, 17851–17862. 10.3748/wjg.v20.i47.17851. [PubMed: 25548483]

66. Lujambio A, Akkari L, Simon J, Grace D, Tschaharganeh DF, Bolden JE, Zhao Z, Thapar V, Joyce JA, Krizhanovsky V, and Lowe SW (2013). Non-cell-autonomous tumor suppression by p53. Cell 153, 449–460. 10.1016/j.cell.2013.03.020. [PubMed: 23562644]

67. Mazzoni M, Mauro G, Erreni M, Romeo P, Minna E, Vizioli MG, Belgiovine C, Rizzetti MG, Pagliardini S, Avigni R, et al. (2019). Senescent thyrocytes and thyroid tumor cells induce M2-like macrophage polarization of human monocytes via a PGE2-dependent mechanism. J Exp Clin Cancer Res 38, 208. 10.1186/s13046-019-1198-8. [PubMed: 31113465]

68. Chen CW, Guan BJ, Alzahrani MR, Gao Z, Gao L, Bracey S, Wu J, Mbow CA, Jobava R, Haataja L, et al. (2022). Adaptation to chronic ER stress enforces pancreatic beta-cell plasticity. Nat Commun 13, 4621. 10.1038/s41467-022-32425-7. [PubMed: 35941159]

69. Hohmeier HE, Mulder H, Chen G, Henkel-Rieger R, Prentki M, and Newgard CB (2000). Isolation of INS-1-derived cell lines with robust ATP-sensitive K+ channel-dependent and -independent glucose-stimulated insulin secretion. Diabetes 49, 424–430. 10.2337/diabetes.49.3.424. [PubMed: 10868964]

70. Ravassard P, Hazhouz Y, Pechberty S, Bricout-Neveu E, Armanet M, Czernichow P, and Scharfmann R (2011). A genetically engineered human pancreatic beta cell line exhibiting glucose-inducible insulin secretion. J Clin Invest 121, 3589–3597. 10.1172/JCI58447. [PubMed: 21865645]

71. Cao W, Yang Y, Wang Z, Liu A, Fang L, Wu F, Hong J, Shi Y, Leung S, Dong C, and Zhang JZ (2011). Leukemia inhibitory factor inhibits T helper 17 cell differentiation and confers treatment effects of neural progenitor cell therapy in autoimmune disease. Immunity 35, 273–284. 10.1016/j.immuni.2011.06.011. [PubMed: 21835648]

72. Schindelin J, Arganda-Carreras I, Frise E, Kaynig V, Longair M, Pietzsch T, Preibisch S, Rueden C, Saalfeld S, Schmid B, et al. (2012). Fiji: an open-source platform for biological-image analysis. Nat Methods 9, 676–682. 10.1038/nmeth.2019. [PubMed: 22743772]

73. Lee H, and Engin F (2020). Preparing Highly Viable Single-Cell Suspensions from Mouse Pancreatic Islets for Single-Cell RNA Sequencing. STAR Protoc 1, 100144. 10.1016/j.xpro.2020.100144. [PubMed: 33377038]

74. Helman A, Klochendler A, Azazmeh N, Gabai Y, Horwitz E, Anzi S, Swisa A, Condiotti R, Granit RZ, Nevo Y, et al. (2016). p16(Ink4a)-induced senescence of pancreatic beta cells enhances insulin secretion. Nat Med 22, 412–420. 10.1038/nm.4054. [PubMed: 26950362]

75. Ray A, and Dittel BN (2010). Isolation of mouse peritoneal cavity cells. J Vis Exp. 10.3791/1488.

76. Justus CR, Leffler N, Ruiz-Echevarria M, and Yang LV (2014). In vitro cell migration and invasion assays. J Vis Exp. 10.3791/51046.

77. Qiu X, Mao Q, Tang Y, Wang L, Chawla R, Pliner HA, and Trapnell C (2017). Reversed graph embedding resolves complex single-cell trajectories. Nat Methods 14, 979–982. 10.1038/nmeth.4402. [PubMed: 28825705]

78. Stuart T, Butler A, Hoffman P, Hafemeister C, Papalexi E, Mauck WM 3rd, Hao Y, Stoeckius M, Smibert P, and Satija R (2019). Comprehensive Integration of Single-Cell Data. Cell 177, 1888–1902 e1821. 10.1016/j.cell.2019.05.031. [PubMed: 31178118]

Context and Significance

Type 1 diabetes (T1D) develops when the body's own immune system kills the insulin-producing pancreatic β-cells. The adaptive mechanisms that can enhance β-cell survival during autoimmune progression remain unclear. Lee et al. from the University of Wisconsin-Madison show that deletion of the unfolded protein response (UPR) genes, ATF6 or IRE1α, in β-cells of a type 1 diabetes (T1D) mouse model before immune cell invasion triggers early senescence leading to changes in β-cell secretome and recruitment of M2 macrophages to pancreatic islets. M2 macrophages mediate anti-inflammatory responses and immune surveillance that promote clearance of terminally senesced β-cells, reduction of β-cell inflammation, and protection against T1D. These results uncover a novel link between the UPR and senescence and suggest that stress-induced adaptive mechanisms may be utilized as a potential preventive strategy for T1D in at-risk individuals.

Highlights

- ATF6 and IRE1α deletion in NOD β-cells before insulitis triggers early senescence
- p21-mediated secretome induces recruitment of M2 macrophages to the islets
- ATF6 and IRE1α deficiency reduces terminal β-cell senescence and diabetes incidence
- Early senescence signature is conserved in residual β-cells of T1D patients

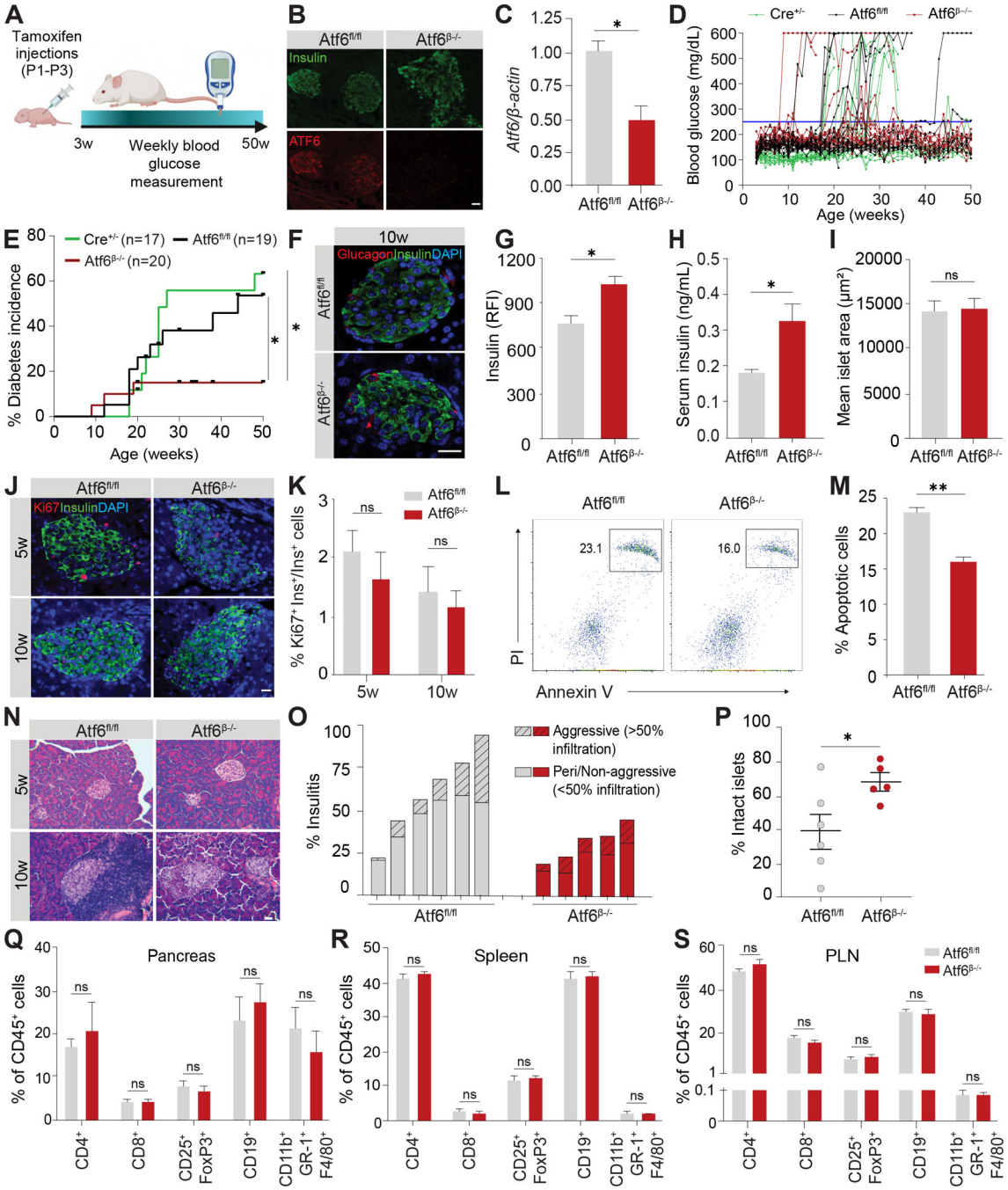

Figure 1. Atf6 deletion in NOD β-cells protects against T1D

(A) Schematic representation of Atf6 deletion.

(B) Insulin and ATF6 co-staining in pancreatic sections from 4–5-week-old Atf6$^{fl/fl}$ and Atf6$^{\beta-/-}$ mice.

(C) RT-qPCR of *Atf6* in the islets of 6-week-old Atf6$^{fl/fl}$ and Atf6$^{\beta-/-}$ mice (n=3/group).

(D and E) (D) Blood glucose measurements and (E) diabetes progression in mice. Blue line denotes 250 mg/dL.

(F) Representative images of insulin, glucagon, and DAPI co-staining of pancreatic sections of 10-week-old $Atf6^{fl/fl}$ (n=8) and $Atf6^{\beta-/-}$ (n=5) mice.
(G) Quantification of insulin RFI.
(H) Serum insulin of 13-week-old mice (n=4–5/group).
(I) Quantification of mean islet area (75–100 islets/animal).
(J and K) (J) Representative images and (K) quantification of insulin, Ki67, and DAPI co-staining (n=5/group).
(L and M) (L) Representative dot plots of Annexin V and PI co-staining of the islets from 19-weekold $Atf6^{fl/fl}$ (n=3) and $Atf6^{\beta-/-}$ (n=5) mice and (M) quantification of apoptotic cells.
(N) Representative H&E images.
(O and P) (O) Percent islet infiltration in 10-week-old $Atf6^{fl/fl}$ (n=6) and $Atf6^{\beta-/-}$ (n=5) mice and (P) percent intact islets.
(Q-S) Immunophenotyping of (Q) pancreas, (R) spleen and (S) PLN of 12-week-old $Atf6^{fl/fl}$ (n=6) and $Atf6^{\beta-/-}$ (n=4) mice. Scale bars: 20μm. RFI, relative fluorescence intensity; w, weeks; ns, not significant; PLN, pancreatic lymph node. Data are represented as mean ± SEM. *p<0.05, **p<0.01. Unpaired, two-tailed t-tests ([C], [G]-[I], [K], [M], [P]-[S]) and Kaplan-Meier estimate [E].

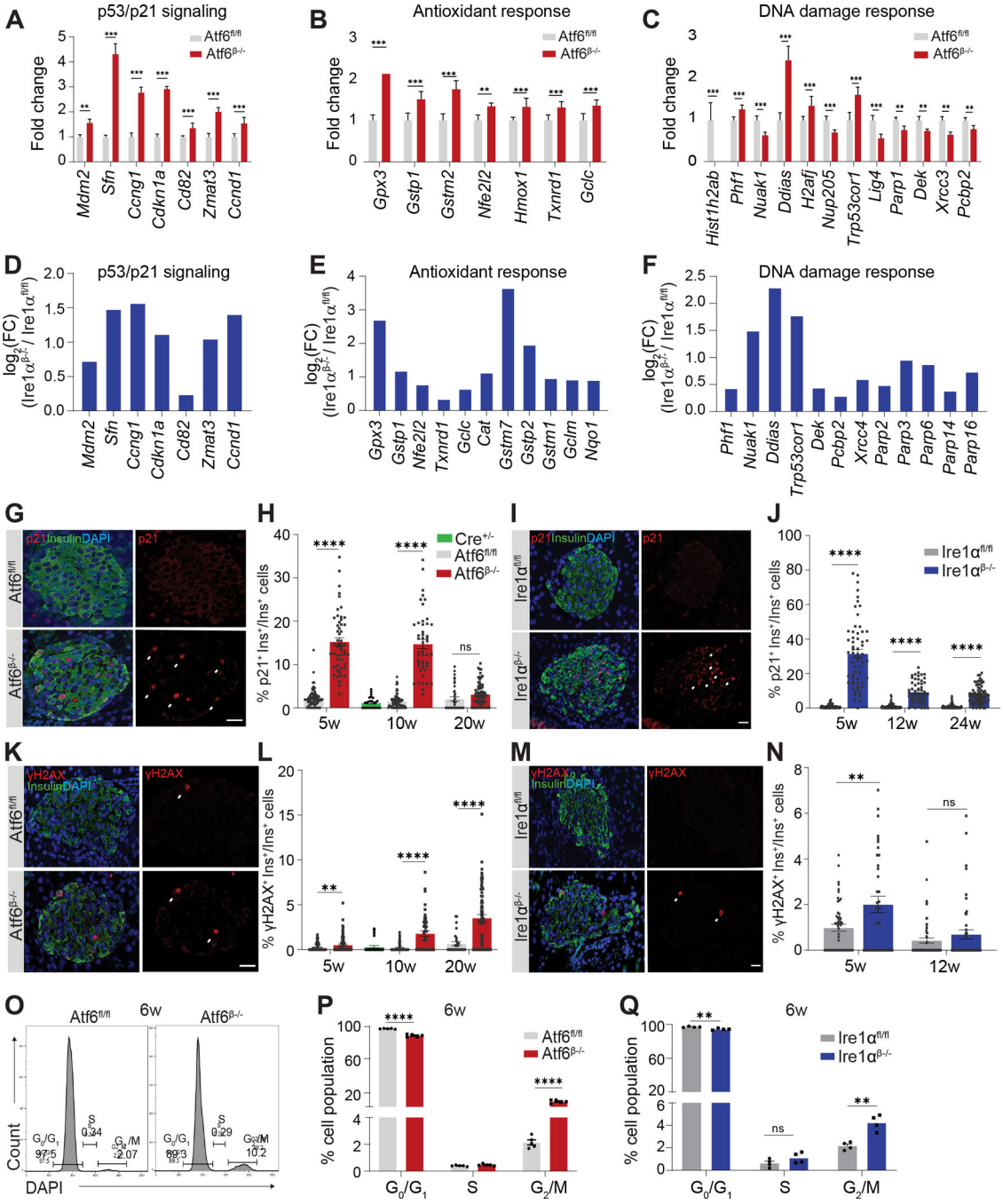

Figure 2. Atf6$^{\beta-/-}$ and Ire1α$^{\beta-/-}$ mice exhibit p21-mediated early senescence

(A-F) (A-C) Expression of genes in the p53/p21 signaling, antioxidant, and DDR pathways from RNA-seq of sorted β-cells from 6-week-old Atf6$^{\beta-/-}$ mice and (D-F) scRNA-seq of islets from 5week-old Ire1α$^{\beta-/-}$ mice, compared to control mice.

(G-J) Insulin, p21, and DAPI co-staining and quantification in pancreatic sections from (G and H) Atf6$^{fl/fl}$, Atf6$^{\beta-/-}$ (n=6/time point), and Ins2Cre$^{ERT/+}$ (n=3) mice, and (I and J) Ire1α$^{fl/fl}$ and Ire1α$^{\beta-/-}$ mice (n=5/time point) at indicated time points.

(K-N) Insulin, γ-H2AX, and DAPI co-staining and quantification in pancreatic sections from (K and L) $Atf6^{fl/fl}$, $Atf6^{\beta-/-}$ (n=6/time point), and $Ins2Cre^{ERT/+}$ (n=3) mice, and (M and N) $Ire1\alpha^{fl/fl}$ and $Ire1\alpha^{\beta-/-}$ mice (n=5/time point) at indicated time points.
(O) Representative histograms of DAPI staining.
(P and Q) Cell cycle analysis of islet cells from 6-week-old (P) $Atf6^{fl/fl}$ and $Atf6^{\beta-/-}$ (n=5/group) mice and (Q) $Ire1\alpha^{fl/fl}$ and $Ire1\alpha^{\beta-/-}$ mice (n=4/group). Scale bars: 20μm.
FC, fold change; w, weeks; ns, not significant. Data are represented as mean ± SEM. **p<0.01, ***p<0.001, ****p<0.0001. Unpaired, two-tailed t-tests ([H], [J], [L], [N], [P], [Q]). FDR<0.05.

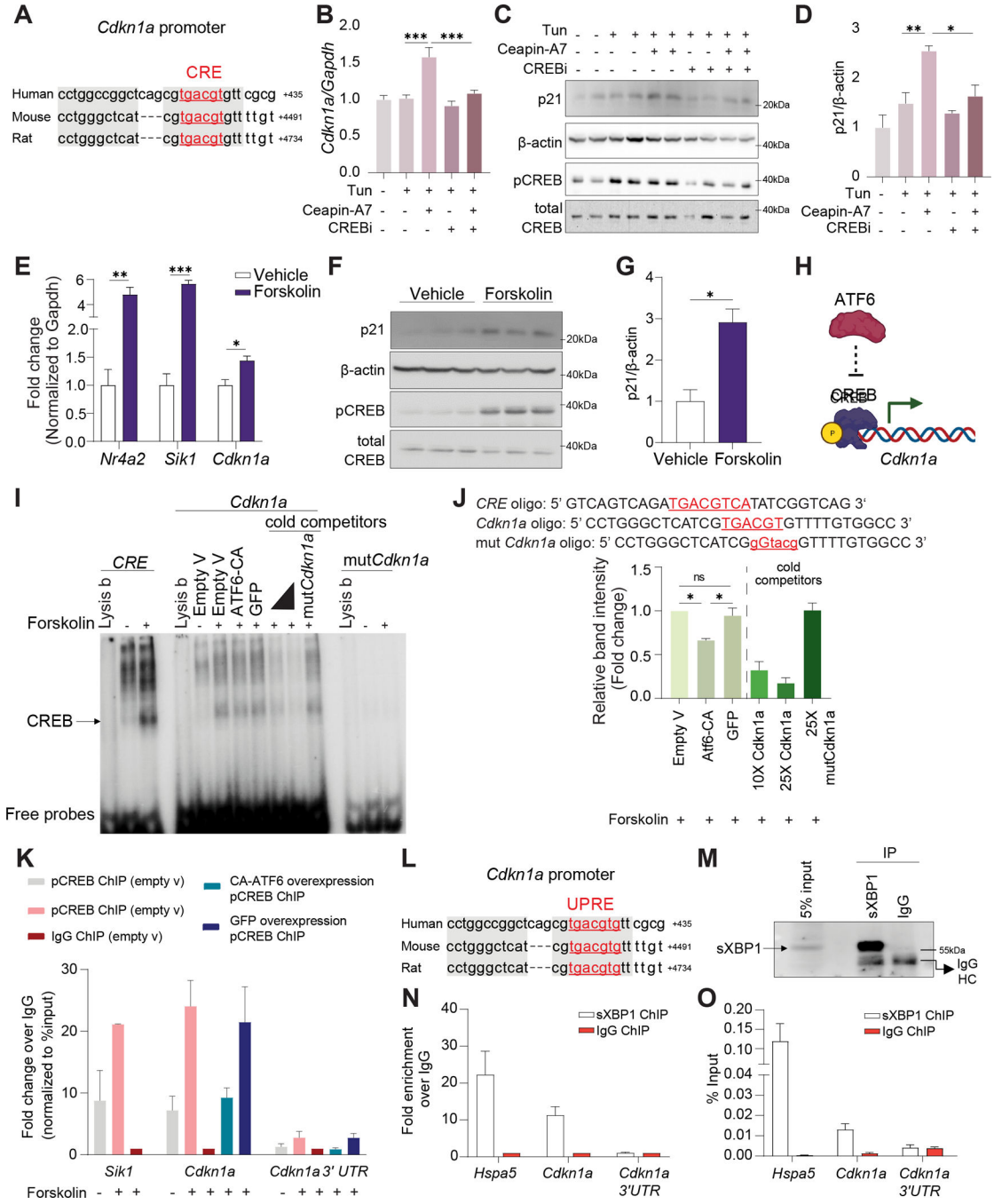

Figure 3. ATF6 and IRE1α/XBP1 differentially regulate p21

(A) Identification of CRE element at *Cdkn1a* promoter of human, mouse, and rat.

(B-D) (B) *Cdkn1a* mRNA levels following 8 hours and (C and D) p21 protein levels following 16 hours in INS1 832/3 cells treated with 2μg/ml tunicamycin (Tun), 15μM Ceapin-A7 and 1μM CREB inhibitor (CREBi), 666–15.

(E-G) (E) mRNA levels of canonical CREB targets and *Cdkn1a,* and (F and G) p21 protein levels in INS1 832/3 cells following 20μM forskolin treatment for 6 hours.

(H) Model for regulation of *Cdkn1a* expression.

(I and J) (I) Representative blot and (J) quantification of EMSA of *Cdkn1a* promoter oligo following incubation with nuclear extracts from transfected and treated INS1 832/3 cells as depicted.

(K) pCREB ChIP-qPCR for *Cdkn1a* promoter in INS1 832/2 cells transfected with empty vector, CA-ATF6, or GFP and treated with 20μM forskolin for 6 hours (n=2 independent experiments).

(L) Identification of UPRE element at *Cdkn1a* promoter of human, mouse, and rat.

(M) Representative image of IP of sXBP1 in INS1 832/3 cells.

(N and O) sXBP1 and IgG ChIP-qPCR for *Cdkn1a* promoter (n=2 independent experiments). Ns, not significant. Data are represented as mean ± SEM. *p<0.05, **p<0.01, ***p<0.001. Unpaired, two-tailed t-tests ([E], [G]) and one-way ANOVA followed by Tukey's post-hoc pair-wise comparisons ([B], [D], [J]).

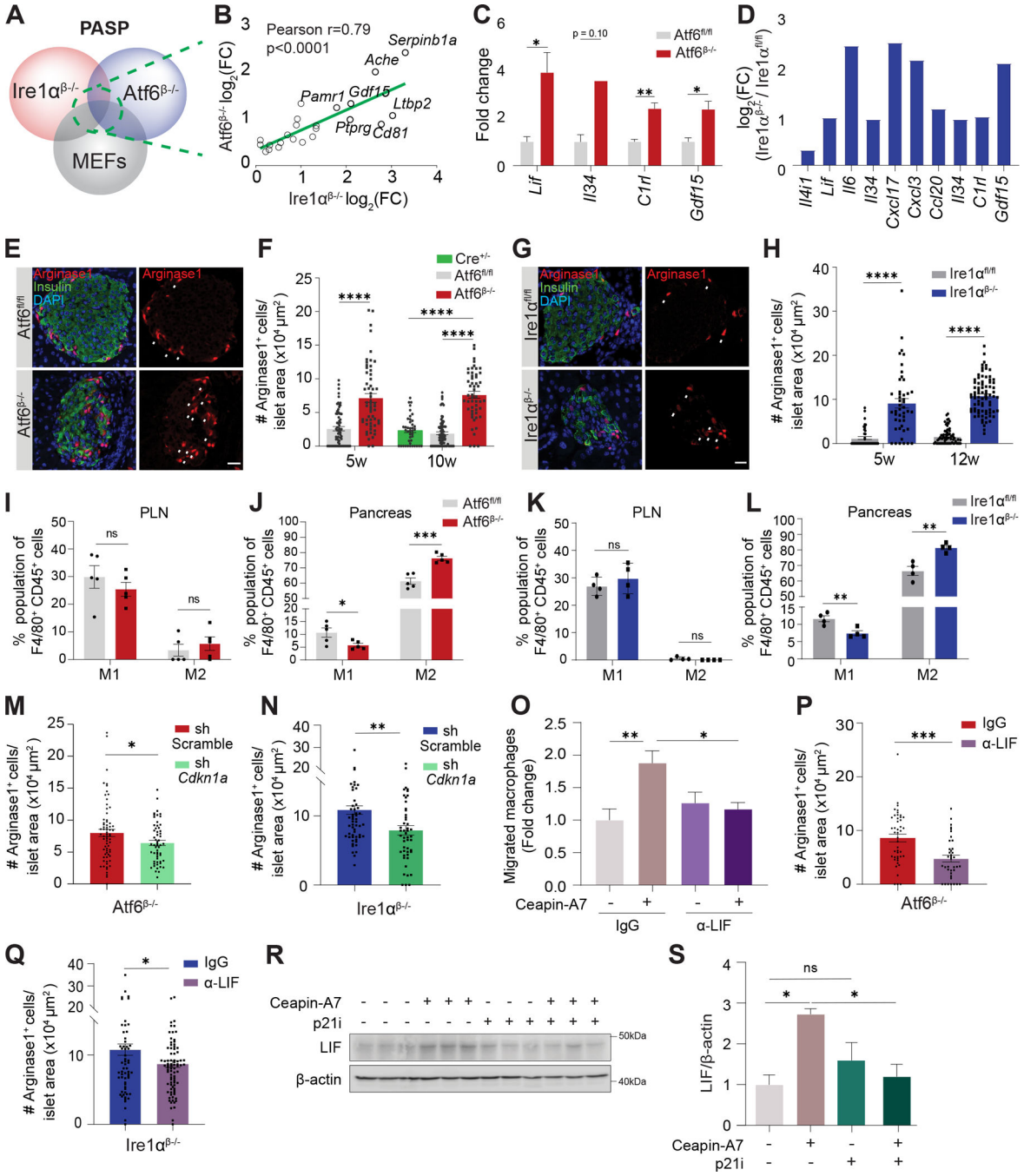

Figure 4. M2 macrophage recruitment to the islets of UPR-deficient mice

(A) Comparison of PASP genes using RNA-seq datasets from Atf6$^{\beta-/-}$, Ire1α$^{\beta-/-}$ mice, and a published gene set from MEF cells.

(B) Correlation of PASP genes between Atf6$^{\beta-/-}$ and Ire1α$^{\beta-/-}$ mice.

(C and D) mRNA levels of macrophage attractants in (C) Atf6$^{\beta-/-}$ and (D) Ire1α$^{\beta-/-}$ β-cells based on RNA-seq analysis.

(E-H) (E and G) Representative images and (F and H) quantification of Arginase1, insulin, and DAPI co-staining in pancreatic sections from 5- and 10-week-old $Atf6^{fl/fl}$ (n=5) and $Atf6^{\beta-/-}$ (n=6) mice, and 5- and 12-week-old $Ire1\alpha^{fl/fl}$ and $Ire1\alpha^{\beta-/-}$ mice (n=5/group).
(I-L) Quantification of M1/M2 macrophages via flow cytometry in (I and K) PLN and (J and L) pancreas from 5-week-old $Atf6^{fl/fl}$ and $Atf6^{\beta-/-}$ (n=5/group) and $Ire1\alpha^{fl/fl}$ and $Ire1\alpha^{\beta-/-}$ mice (n=4/group).
(M and N) Quantification of Arginase1, insulin, and DAPI co-staining in pancreatic sections from 5-week-old (M) $Atf6^{\beta-/-}$ (n=5/group) and (N) $Ire1\alpha^{\beta-/-}$ mice (n=4/group) following shScramble or sh*Cdkn1a* transduction.
(O) Quantification of migrated macrophages in the presence of CM from NIT1 cells that were incubated with α-LIF or control IgG.
(P and Q) Quantification of Arginase1, insulin, and DAPI co-staining following LIF neutralization from 5-week-old (P) $Atf6^{\beta-/-}$ (n=5/group) and (Q) $Ire1\alpha^{\beta-/-}$ mice (n=3 for IgG, n=4 for α-LIF).
(R and S) (R) Representative western blot image and (S) quantification of LIF expression in NIT1 cells. Scale bars: 20μm. CM, conditioned media; PLN, pancreatic lymph node; w, weeks; ns, not significant. Data are represented as mean ± SEM. *p<0.05, **p<0.01, ***p<0.001, ****p<0.0001. FDR<0.05. Unpaired, two-tailed t-tests ([F],[H-N],[P-Q]) and one-way ANOVA followed by Tukey's post-hoc pair-wise comparisons ([O], [S]).

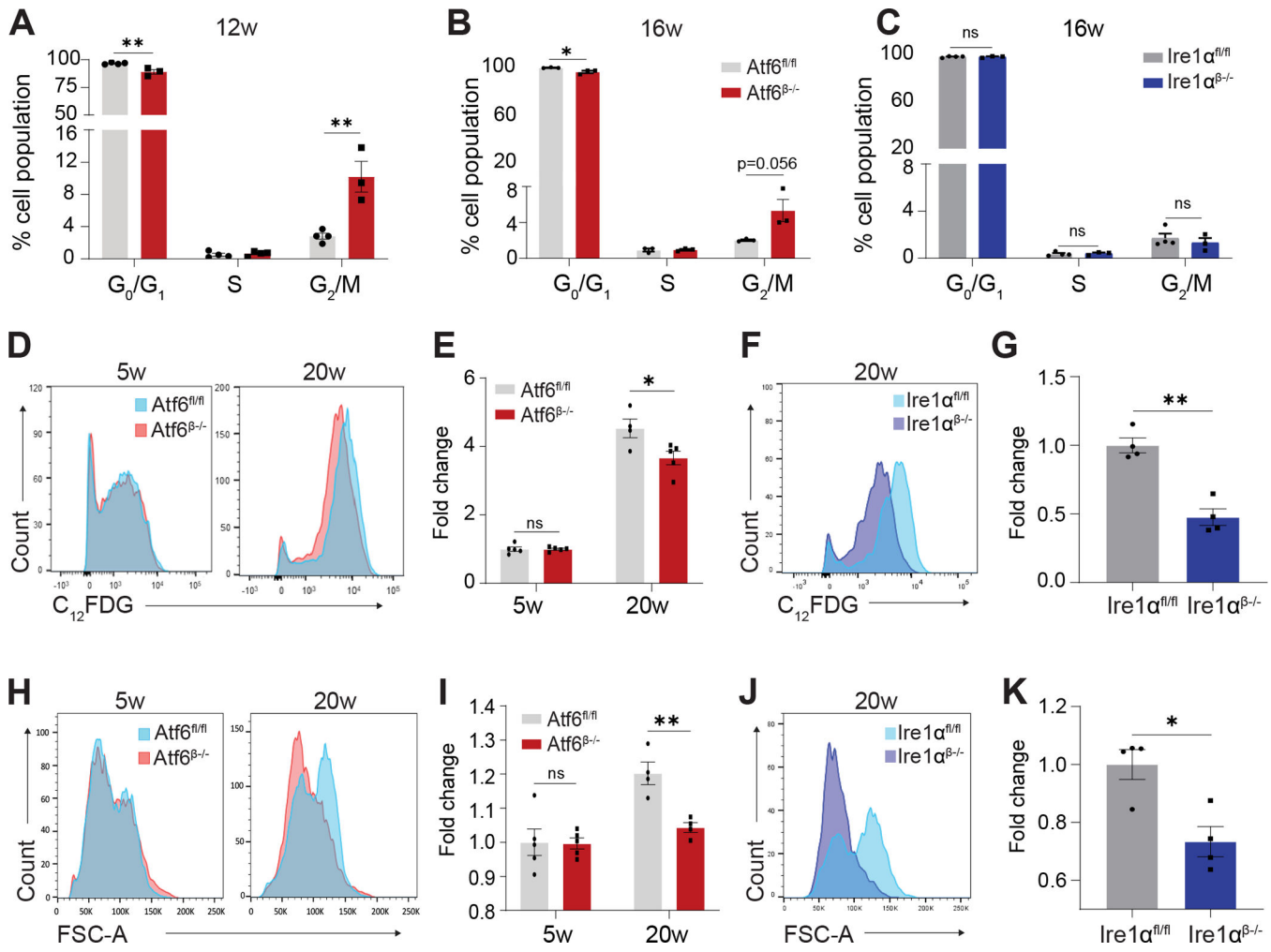

Figure 5. β-Cells of Atf6$^{β-/-}$ and Ire1α$^{β-/-}$ mice exhibit significantly less terminal senescence

(A-C) Cell cycle analysis of islet cells from (A) 12- and (B) 16-week-old Atf6$^{fl/fl}$ and Atf6$^{β-/-}$ mice (n=3–4/group), and (C) 16-week-old Ire1α$^{fl/fl}$ (n=4) and Ire1α$^{β-/-}$ (n=3) mice by flow cytometry.

(D and E) (D) Representative histogram of C_{12}FDG staining and (E) its quantification in islets from 5- and 20-week-old Atf6$^{fl/fl}$ and Atf6$^{β-/-}$ mice (n=5/group/time point).

(F and G) (F) Representative histogram of C_{12}FDG staining and (G) its quantification in islets from 20-week-old Ire1α$^{fl/fl}$ and Ire1α$^{β-/-}$ mice (n=4/group).

(H and I) (H) Representative histogram of cell size and (I) its quantification in islets from 5- and 20-week-old Atf6$^{fl/fl}$ and Atf6$^{β-/-}$ mice.

(J and K) (J) Representative histogram of cell size and (K) its quantification in islets from 20-week-old Ire1α$^{fl/fl}$ and Ire1α$^{β-/-}$ mice (n=4/group). C_{12}FDG, 5-Dodecanoylaminofluorescein Di-β-D-Galactopyranoside; w, weeks; ns, not significant. Data are represented as mean ± SEM. *p<0.05, **p<0.01. Unpaired, two-tailed t-tests ([A], [B], [C], [E], [G], [I], [K]).

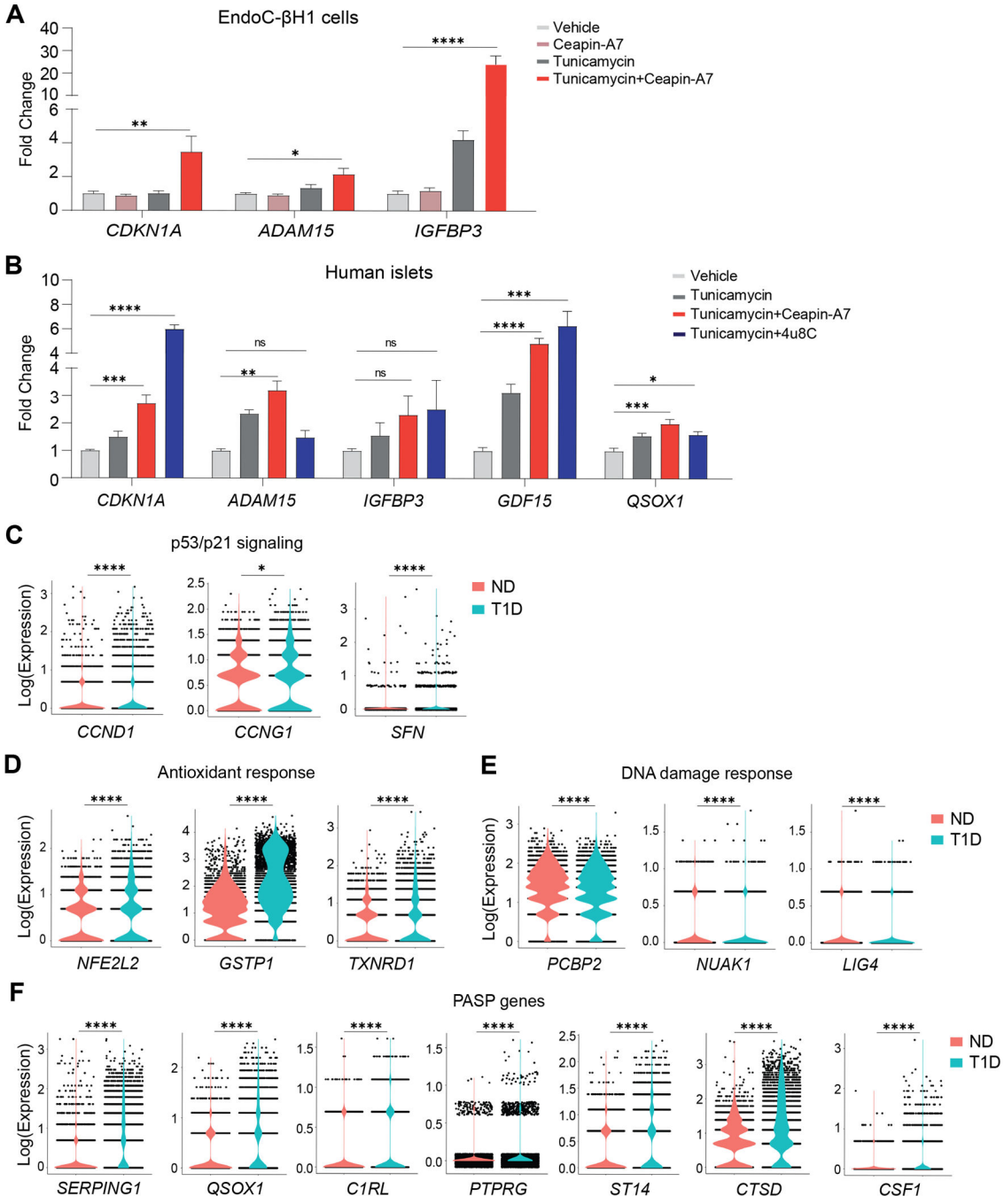

Figure 6. Early senescence signature of UPR-deficient mice is preserved in residual β-cells of T1D donors

(A and B) qPCR analysis of PASP gene expression in (A) EndoC-βH1 cells, following 2.5 μg/mL tunicamycin and 15μM Ceapin-A7 treatments for 72 hours, and (B) islets obtained from healthy donors following 0.25μg/ml tunicamycin, 15μM Ceapin-A7, and 50μM 4μ8C treatments for 72 hours (n=3 male donors).

(C-F) Log expression analysis of (C) p53/p21 signaling pathway, (D) antioxidant response, (E) DDR, and (F) PASP genes in individuals with no-diabetes (ND) (n=5) and T1D (n=6). Expression is normalized read counts. ns, not significant. Data are represented as means

± SEM. *p<0.05, **p<0.01, ***p<0.001, ****p<0.0001. One-way ANOVA followed by Tukey's post-hoc pair-wise comparisons ([A], [B]) and Wilcoxon–Mann–Whitney test ([C], [D], [E], [F]).

Key resources table

REAGENT or RESOURCE	SOURCE	IDENTIFIER
Antibodies		
Guinea pig anti-insulin (1:200)	Linco Research	Cat# 4011-01; RRID: AB_433702
Rabbit polyclonal anti-glucagon (1:100)	Cell Signaling Technology	Cat# 2760S; RRID: AB_659831
Rabbit monoclonal anti-Ki67 (1:100)	Cell Signaling Technology	Cat# 9129; RRID: AB_2687446
Goat anti-Guinea Pig IgG (H+L) Highly CrossAdsorbed Secondary Antibody, Alexa Fluor 488 (1:200)	ThermoFisher	Cat# A-11073; RRID: AB_2534117
Goat anti-Rabbit IgG (H+L) Highly Cross-Adsorbed Secondary Antibody, Alexa Fluor 568 (1:200)	ThermoFisher	Cat# A-11036; RRID: AB_10563566
TruStain FcX (anti-mouse CD16/32) (1:10)	Biolegend	Cat# 101319; RRID: AB_1574973
Brilliant Violet 421 anti-mouse CD3 (1:100)	Biolegend	Cat# 100228; RRID: AB_2562553
FITC anti-mouse/human CD11b (1:100)	Biolegend	Cat# 101205; RRID: AB_312788
Brilliant Violet 785 anti-mouse CD45 (1:100)	Biolegend	Cat# 103149; RRID: AB_2564590
APC anti-mouse F4/80 (1:100)	Biolegend	Cat# 123116; RRID: AB_893481
PerCP/Cyanine5.5 anti-mouse Ly-6G/Ly-6C (Gr1) (1:100)	Biolegend	Cat# 108427; RRID: AB_893561
Brilliant Violet 421 anti-mouse CD45 (1:100)	Biolegend	Cat# 103134; RRID: AB_2562559
Brilliant Violet 785 anti-mouse CD8a (1:100)	Biolegend	Cat# 100749; RRID: AB_11218801
FITC anti-mouse CD4 (1:100)	Biolegend	Cat# 100510; RRID: AB_312713
PerCP/Cyanine5.5 anti-mouse/human CD11b (1:100)	Biolegend	Cat# 101228; RRID: AB_893232
PE anti-mouse CD25 (1:100)	Biolegend	Cat# 101903; RRID: AB_312846
PE/Dazzle 594 anti-mouse CD19 (1:100)	Biolegend	Cat# 115553; RRID: AB_2564000
PE anti-mouse FOXP3 (1:100)	Biolegend	Cat# 126404; RRID: AB_1089117
PE anti-mouse CD4 (1:100)	Biolegend	Cat# 116005; RRID: AB_313690
FITC anti-mouse CD8a (1:100)	Biolegend	Cat# 100705; RRID: AB_312744
PE anti-mouse CD11c (1:100)	Biolegend	Cat# 117307; RRID: AB_313776
FITC anti-mouse CD206 (1:100)	Biolegend	Cat# 141703; RRID: AB_10900988
Anti-mouse LIF (1:100)	R&D Systems	Cat# AF449; RRID: AB_2136095
Normal goat IgG control (1:100)	R&D Systems	Cat# AB-108-C; RRID: AB_354267
Goat anti-ATF6 (1:50)	Santa Cruz	Cat# SC22799; RRID: AB_2242950
Rabbit anti-p21 (1:100)	Abcam	Cat# ab188224; RRID: AB_2734729
Rabbit anti-phosphohistone H2A.X (1:100)	Cell Signaling	Cat# 9718S; RRID: AB_2118009
BV421 anti-mouse glucagon (1:100)	BD	Cat# 565891; RRID: AB_2739385
APC anti-mouse insulin (1:100)	R&D Systems	Cat# IC1417A; RRID: AB_2126535
Mouse anti-pCREB1 (1:200)	Santa Cruz	Cat# sc-81486; RRID: AB_1125727
Rabbit anti-CREB (1:1000)	Millipore	Cat# 06-863; RRID: AB_310268
Mouse anti-p21 (1:200)	Santa Cruz	Cat# sc-53870; RRID: AB_785026
Mouse anti-β-actin HRP (1:2500)	Santa Cruz	Cat# sc-47778; RRID: AB_626632
Rabbit anti-Arginase1 (1:100)	Cell Signaling	Cat# 93668; RRID: AB_2800207
Rabbit anti-NRF2 (1:1000)	Cell Signaling	Cat# 12721; RRID: AB_2715528

REAGENT or RESOURCE	SOURCE	IDENTIFIER
Rabbit anti-Cleaved Caspase-3 (1:1000)	Cell Signaling	Cat# 9661; RRID: AB_2341188
Anti-rabbit IgG, HRP-linked Antibody (1:2500)	Cell Signaling	Cat# 7074; RRID: AB_2099233
Anti-mouse IgG, HRP-linked Antibody (1:3000)	Cell Signaling	Cat# 7076; RRID: AB_330924
Rabbit IgG control (1:7000)	Cell Signaling	Cat# 3900; RRID: AB_1550038
Rabbit anti-sXBP1 (1:200)	Cell Signaling	Cat# 82914
Mouse anti-GFP (1:100)	Santa Cruz	Cat# sc-9996; RRID: AB_627695
Bacterial and virus strains		
AAV8-RIP-GFP-shCdkn1a	VectorBuilder	Vector ID: VB220330-1271yha
AAV8-CMV-GFP-shScramble	VectorBuilder	Vector ID: VB010000-9397wgw
Biological samples		
Mouse islets and pancreatic sections	In house procedure	For information contact Feyza Engin
Human donor islets	Integrated Islet Distribution Program	See Table S2
Chemicals, peptides, and recombinant proteins		
Collagenase	Sigma	Cat# C7657
Histopaque (1.077 g/mL)	Sigma	Cat# 10771
Ghost Dye Red 780	Tonbo Biosciences	Cat# 13-0865
Accutase	Innovative Cell Technologies	Cat# AT-104
Vibrance antifade mounting medium with DAPI	Vector Laboratories	Cat# H-1800
Tamoxifen	Sigma	Cat# T5648
ACK lysing buffer	ThermoFisher	Cat# A1049201
Power SYBR Green PCR Master Mix	ThermoFisher	Cat# 4367659
Fetal bovine serum	ThermoFisher	Cat# F0926
Bovine serum albumin	Sigma	Cat# A7888
Normal goat serum	ThermoFisher	Cat# 50413254
Tunicamycin	Sigma	Cat# T7765
Ceapin-A7	Sigma	Cat# SML2330
Forskolin	Cayman	Cat# 11018
UC2288	Sigma	Cat# 532813
666-15	MedChem	Cat# HY-101120
4μ8C	Sigma	Cat# SML0949
C_{12}FDG	Cayman	Cat# 25583
DAPI	Biolegend	Cat# 422801
RNasin ribonuclease inhibitor	Promega	Cat# N2615
SuperSignal West Pico Plus	ThermoFisher	Cat# 34577
SuperScript II Reverse Transcriptase	ThermoFisher	Cat# 18064014
TRIzol Reagent	ThermoFisher	Cat# 15596026
Protease inhibitor cocktail	Sigma	Cat# P8340

REAGENT or RESOURCE	SOURCE	IDENTIFIER
RNase A	ThermoFisher	Cat# EN0531
Proteinase K	ThermoFisher	Cat# EO0491
Lipofectamine 2000	ThermoFisher	Cat# 11668019
Critical commercial assays		
Mouse Ultrasensitive Insulin ELISA	Alpco	Cat# 80-INSMSU-E01
High-Capacity cDNA Reverse Transcription Kit with RNase Inhibitor	ThermoFisher	Cat# 4374966
Agilent RNA 6000 Nano Kit	Agilent	Cat# 5067-1511
Agilent DNA 1000 Kit	Agilent	Cat# 5067-1504
Qubit RNA HS Assay Kit	ThermoFisher	Cat# Q32852
TruSeq Stranded Total RNA (Human/Mouse/Rat)	Illumina	Cat# 20020597
Qubit dsDNA HS Assay Kit	ThermoFisher	Cat# Q32851
RNeasy Plus Mini Kit	Qiagen	Cat# 74134
FITC Annexin V Apoptosis Detection Kit with PI	Biolegend	Cat# 640914
Mouse CXCL14 ELISA Kit	RayBiotech	Cat# ELM-CXCL14
RNeasy Micro Kit	Qiagen	Cat# 74004
RecoverAll Total Nucleic Acid Isolation Kit	Invitrogen	Cat# AM1975
TURBO DNA-free Kit	Invitrogen	Cat# AM1907
Nuclear Extraction Kit	Cayman	Cat# 10009277
BCA Protein Assay Kit	ThermoFisher	Cat# 23227
Deposited data		
Single cell Ire1α RNA-seq data	Lee et al., 2020	GEO: GSE144471
Sorted β-cell Atf6 RNA-seq data	This paper	GEO: GSE239947
Single cell RNA-seq data	The Human Pancreas Analysis Program - HPAP	HPAP-019
Single cell RNA-seq data	The Human Pancreas Analysis Program – HPAP	HPAP-022
Single cell RNA-seq data	The Human Pancreas Analysis Program – HPAP	HPAP-024
Single cell RNA-seq data	The Human Pancreas Analysis Program – HPAP	HPAP-026
Single cell RNA-seq data	The Human Pancreas Analysis Program – HPAP	HPAP-029
Single cell RNA-seq data	The Human Pancreas Analysis Program – HPAP	HPAP-020
Single cell RNA-seq data	The Human Pancreas Analysis Program – HPAP	HPAP-021
Single cell RNA-seq data	The Human Pancreas Analysis Program – HPAP	HPAP-023
Single cell RNA-seq data	The Human Pancreas Analysis Program – HPAP	HPAP-028
Single cell RNA-seq data	The Human Pancreas Analysis Program – HPAP	HPAP-032

REAGENT or RESOURCE	SOURCE	IDENTIFIER
Single cell RNA-seq data	The Human Pancreas Analysis Program - HPAP	HPAP-055
Experimental models: Cell lines		
INS1 823/3	Hohmeier et al., 2000	RRID: CVCL_ZL55
NIT1	ATCC	Cat# CRL-2055
EndoC-βH1	Ravassard et al., 2011	RRID: CVCL_L909
Experimental models: Organisms/strains		
Mouse: NOD Tg(Ins2-cre/ERT)1Dam/J	Lee et al., 2020	N/A
Mouse: NOD Ire1α$^{fl/fl}$	Lee et al., 2020	N/A
Mouse: Atf6$^{fl/fl}$	Engin et al., 2013	N/A
Mouse: NOD Atf6$^{fl/fl}$	This paper	N/A
Oligonucleotides		
Primers for qPCR, see Table S4	Integrated DNA Technologies	N/A
EMSA CRE oligo: GTCAGTCAGATGACGTCATATCGGTCAG	Integrated DNA Technologies	N/A
EMSA *Cdkn1a* oligo: GTCAGTCAGATGACGTCATATCGGTCAG	Integrated DNA Technologies	N/A
EMSA mutant *Cdkn1a* oligo: CCTGGGCTCATCGGGTACGGTTTTGTGGCC	Integrated DNA Technologies	N/A
Primer: ChIP *Cdkn1a*: F: GGCTCATCGTGACGTGTTT R: CAAGGAGTGGTGAGTCAGTTTC	Integrated DNA Technologies	N/A
Primer: ChIP *Cdkn1a* 3' UTR: F: GAAGGGAACGGGTACACAGG R: ACACACACAGGGATGCTCTG	Integrated DNA Technologies	N/A
Primer: ChIP *Hspa5*: F: GTCCAGGCTGGTGTCCTCTC R: GATTATCGGAAGCCGTGGAG	Integrated DNA Technologies	N/A
Recombinant DNA		
Plasmid: CMV-GFP	Laboratory of Judith Simcox	N/A
Plasmid: 3XFlag-CA-Atf6	This paper	N/A
Plasmid: CA-Atf6	This paper	N/A
Software and algorithms		
GraphPad Prism v8-10	GraphPad Software	https://www.graphpad.com/
Fiji	Schindelin et al., 2012	https://imagej.net/software/fiji/downloads
FlowJo v10	FlowJo, LLC	https://www.flowjo.com
FACSDiva v3.0	BD Biosciences	N/A
Monocle v2.8.0	Qiu et al., 2017	https://cole-trapnell-lab.github.io/monocle-release/
Seurat V3	Stuart et al., 2019	https://satijalab.org/
R v3.5.2	RCore Team, R Foundation for Statistical Computing	https://www.r-project.org/

REAGENT or RESOURCE	SOURCE	IDENTIFIER
NIS-Elements	Nikon	N/A
Other		
LSRFortessa X-20	BD Biosciences	N/A
Attune NxT Flow Cytometer	Invitrogen	N/A
A1R+ Confocal	Nikon	N/A
STORM/TIRF/epifluorescence Microscope	Nikon	N/A
HiSeq 2500 System	Illumina	N/A
Countess II Automated Cell Counter	ThermoFisher	Cat# A27977
CONTOUR Next glucometer	Ascensia	N/A
CONTOUR Next test strips	Ascensia	N/A
Typhoon FLA 9500	GE	N/A